



Czech Technical University in Prague

Faculty of Civil Engineering

Department of Hydraulics and Hydrology

CML R-R modelling

Ing. Jaroslav Pastorek

Doctoral study programme:

Stavební inženýrství | Civil Engineering

Branch of study:

Vodní hospodářství a vodní stavby | Water Engineering and Water Management

Supervisor:

Ing. Vojtěch Bareš, Ph.D.

January 2021

Declaration

I hereby declare that this thesis has been composed by myself under the guidance of the supervisor Ing. Vojtěch Bareš, Ph.D.

I confirm that the thesis submitted is my own work and effort, except where work which has formed part of jointly-authored publications is included. My contribution and those of the other authors to such work are explicitly indicated in the thesis.

Any additional sources of information from which I have quoted or drawn reference have been referenced fully in the text and in the list of references.

.....
Jaroslav Pastorek

Acknowledgements

I would like to thank everyone who supported my work on this project. In particular, I would like to thank Vojtěch Bareš, Martin Fencl, and David Stránský from CTU in Prague, and also Jörg Rieckermann, Andreas Scheidegger, and others from Eawag.

I would also like to thank T-Mobile Czech Republic, a.s., for providing the CML data, and especially Pavel Kubík for assisting with our numerous requests. I would also like to thank Pražská vodohospodářská společnost, a.s., for providing rainfall data from their rain gauge network, and Pražské vodovody a kanalizace, a.s., for carefully maintaining the flow meter and the rain gauges inside the experimental catchment.

I would like to thank the team around the `ctuthesis` L^AT_EX package which provided a template for this document.

The work on the thesis was supported by:

- the Czech Science Foundation under the projects no.
 - 14-22978S
 - 17-16389S
 - 20-14151J
- the Grant Agency of the Czech Technical University in Prague under the projects no.
 - SGS16/057/OHK1/1T/11
 - SGS17/064/OHK1/1T/11
 - SGS18/053/OHK1/1T/11
 - SGS19/045/OHK1/1T/11
 - SGS20/050/OHK1/1T/11

I owe a special thank you to Deep Thought for the answer to the ultimate question of life, the universe, and everything.

Abstract

We develop ...

Keywords:

Abstrakt

Rozvíjíme ...

Klíčová slova:

Překlad názvu: nejaký český text

Contents

1 Introduction	1	5 The effect of link characteristics and their position on runoff simulations	37
1.1 Objectives of the thesis	1	5.1 Introduction	37
1.2 Thesis' structure	1	5.2 Methods	39
2 Theory	3	5.3 Results	41
2.1 Current rainfall monitoring practices	4	5.4 Discussion	47
2.2 Rainfall retrieval from commercial microwave links	5	5.5 Conclusions	49
2.3 CML QPE errors	7		
2.4 Rainfall Data Set Evaluation . . .	11	6 Practical Approaches to Wet-Antenna Correction	51
2.5 Prediction uncertainty quantification in hydrology	13	6.1 Introduction	52
2.6 Explicit statistical consideration of model bias	15	6.2 Methods	53
3 Material	21	6.3 Results	56
3.1 Data retrieval and availability . . .	22	6.4 Discussion	61
3.2 Rainfall-runoff model and its reliability	24	6.5 Conclusions	63
4 On the value of CML QPEs for urban rainfall-runoff modelling: The pilot study	27		
4.1 Introduction	27	7 On the value of CML QPEs for urban rainfall-runoff modelling: The final study	65
4.2 Methods	28	7.1 Methods	65
4.3 Results	33		
4.4 Discussion	36	8 Dummy chapter	67
		9 Conclusion	69
		Bibliography	71

Chapter 1

Introduction

This chapter is about the intorduction.

1.1 Objectives of the thesis

This thesis aims to

? further improve the understanding of the potential of CML QPEs in urban hydrological modelling.

1.2 Thesis' structure

This thesis is structured as follows

Chapter 2

Theory

This chapter is about the theory (?and methods?) relevant for multiple following chapters.

Urban drainage systems are designed to drain waste- and stormwater from land surfaces in urban areas using combined or separate sewer networks. However, excessive amounts of stormwater can overload drainage systems and cause urban pluvial flooding and health risks due to pathogens, decrease the efficiency of wastewater treatment plants, or impact the aquatic biota of receiving waters through hydraulic stress and pollution. Therefore, the operational management of the quantity and quality of urban stormwater runoff is a serious concern in urban environmental management (Tsihrintzis & Hamid, 1997).

Since precipitation is the essential driver of runoff processes in urban areas, rainfall observations are the key input data when designing and operating urban drainage systems during wet weather periods. Nowadays, the mitigation of the negative effects of urban drainage on society and the environment is often related to methods and concepts requiring operational rainfall products which are available in (near) real time and with a high spatial and/or temporal resolution (Einfalt et al., 2004). Such rainfall observations are employed in real-time control strategies to optimize treatment processes at wastewater treatment plants (Schütze et al., 2004), or to minimize the impacts of sewer overflows (Vezzaro & Grum, 2014). Furthermore, these data are used for extreme event analyses, e.g. for the evaluation of insurance damage claims (Spekkers et al., 2013) or for operational warnings (Montesarchio et al., 2009). Operational rainfall data are becoming increasingly important because of the ongoing climate change (van der Pol et al., 2015) as the intensity and frequency of heavy rainfall in many areas around the world are expected to increase (Willems et al., 2012).

2.1 Current rainfall monitoring practices

In general, rainfall data of sufficient quality is lacking for most of the Earth's land surface. To make things worse, coverage by surface precipitation gauging networks has declined in many regions around the world (Lorenz & Kunstmann, 2012). Global precipitation data sets can be obtained from satellite missions, but the accuracy and spatiotemporal resolution of these observations are still insufficient to be used in the hydrological modelling of small, mountainous or urban catchments (Kidd & Huffman, 2011).

The requirements on the temporal and spatial resolution of rainfall data are higher in urban catchments (e.g. Schilling, 1991; Berne et al., 2004) because, hydrologically, they differ from natural ones in two fundamental aspects. Firstly, the scales of areas examined in urban and natural catchment hydrology typically differ in orders of magnitude. Secondly, urban areas are covered by a high ratio of impermeable surfaces that not only limit rainfall infiltration, but also lead to more surface runoff (e.g. causing higher peak flows) and a faster response of the runoff process.

Tipping bucket rain gauges represent the traditional way of retrieving precipitation measurements in urban areas. However, these devices often fail to provide sufficient information on the spatiotemporal variability of rainfall, frequently due to the low densities of rain gauge networks. In particular, when heavy storm events, crucial for the evaluation of urban stormwater systems, are considered, the spatial representativeness of point rainfall observations from rain gauges is limited.

Weather radar observations have been extensively studied in recent years. Due to the inherent limitations of this technology (indirect rainfall measurement, often in relatively high altitudes above the ground and far away from the radar), radar rainfall data are commonly adjusted to rainfall measurements from rain gauges to be more advantageous for hydrological modelling (Harrison et al., 2009). These adjustments usually reduce the mean areal bias of rainfall fields, though often destroy the small-scale spatial structure of local extremes (Wang et al., 2015). However, neglecting rainfall spatiotemporal variability at small scales can lead to substantial errors in the runoff modelling of urban catchments (Gires et al., 2012). The smoothing of local extremes could be reduced by adjusting the radar data to dense rain gauge networks. Nevertheless, it has been concluded that traditionally available rain gauge networks and adjustment techniques do not meet the requirements of urban hydrology (Wang et al., 2013; Borup et al., 2016). Although the usage of weather radars for urban water management applications has been extensively investigated in the past decades and substantial progress has been made towards reliable high-quality data, many challenges remain unresolved. For example, it is difficult to quantify uncertainty arising from the discrepancy

between the catch area of a rain gauge (in the order of 10^{-2} m 2) and the area of a radar pixel (in the order of 10^4 – 10^6 m 2) (e.g. Anagnostou et al., 1999). Similarly, adjusting radar data in an operational mode is both a methodological and technical challenge because rain gauge data are often delivered with a delay. Finally, the availability of weather radars is mostly limited to most developed countries (Heistermann et al., 2013), where, even in these regions, there are observational gaps when radar observations are not available in the desired spatiotemporal resolution.

One possibility to overcome the above challenges could be so-called “opportunistic sensing” (Tauro et al., 2018). Opportunistic precipitation sensing can provide rainfall data from new types of devices which could conveniently complement traditional precipitation observation networks and, thus, improve rainfall data availability. The recent development of various accessible hardware and software solutions has made measurements with special purpose sensors widely available throughout many different fields (Swan, 2012). Furthermore, there are numerous online amateur weather networks that aggregate and visualize citizen-contributed weather observations (Gharesifard et al., 2017; de Vos et al., 2017). However, quality control of such crowdsourced data (and associated metadata) from amateur weather stations is extremely challenging since these devices are often uncalibrated or irregularly maintained. Furthermore, as with radar rainfall observations, this kind of data is primarily available in developed regions only.

Opportunistic sensing of precipitation can also be performed using devices not constructed primarily for rainfall observation (e.g. telecommunication infrastructure or building automation sensors), which are often connected to centralized communication infrastructure, so the data can be queried in (sub-)minute intervals. This is the case of commercial microwave links whose millimeter-wave radio signal is attenuated by rainfall droplets.

2.2 Rainfall retrieval from commercial microwave links

Commercial microwave links (CMLs) are point-to-point radio connections widely used as cellular backhaul. A substantial part of CML networks is operated at frequencies between 20 and 40 GHz where radio wave attenuation caused by raindrops is almost proportional to rainfall intensity. These CMLs can, therefore, be used as unintended rainfall sensors providing path-integrated quantitative precipitation estimates (QPEs). Moreover, CML data are accessible online in real time from network operation centers either through network monitoring systems or specifically designed server-sided applications (Chwala et al., 2016).

2. Theory

Although deriving precipitation estimates from the attenuation of microwaves was originally suggested several decades ago (Atlas & Ulbrich, 1977), the idea has experienced a renaissance in recent years, thanks to the extensive growth of cellular networks (Messer et al., 2006; Leijnse et al., 2007) which frequently incorporate CMLs. Recently, there has been about four million CMLs being used worldwide within cellular networks and the number has been increasing (Ericsson, 2016).

The relationship between raindrop-induced attenuation A_r [dB] and rainfall intensity R [mm/h] is robust and well-understood. For a given rainfall intensity, A_r is proportional to CML length and frequency. The relation can be expressed using the following approximation:

$$R = \alpha(A_r/L)^\beta, \quad (2.1)$$

where L [m] is the length of a given CML, and α [mm/h km $^\beta$ dB $^{-\beta}$] and β [-] are empirical parameters dependent upon CML frequency and polarization, and drop size distribution (Olsen et al., 1978). The fraction A_r/L can be expressed as a single variable – specific raindrop attenuation γ [dB/km].

Nonetheless, A_r must be separated from other components of the difference between the transmitted and received signal levels $TRSL$ [dB], for whose purposes the following relation is often used:

$$TRSL = B + A = B + A_{wa} + A_r \quad (2.2)$$

where B [dB] represents baseline attenuation consisting of, e.g., free space loss and gaseous attenuation, A [dB] stands for observed attenuation after baseline separation (henceforth referred to as “observed attenuation”), and A_{wa} [dB] represents wet antenna attenuation (WAA). Imprecise quantification of the raindrop-induced attenuation A_r due to CML instrumental uncertainties such as WAA estimation represents a major source of errors in CML QPEs (Chwala & Kunstmann, 2019, more details in 2.3.1).

Thanks to the extensive continental coverage of cellular networks, CMLs represent a promising rainfall sensors for hydrological modelling. The greatest potential of this technique is in areas where traditional infrastructure for rainfall measurement is, in general, insufficient (Gosset et al., 2016), e.g. in developing countries. Nevertheless, CMLs might also conveniently complement traditional monitoring networks common in developed countries, since, unlike weather radars, they observe rainfall close to the ground. Moreover, CML rainfall measurements have a path-integrated character which makes them better suited for capturing areal rainfalls over a catchment than rain gauges.

Only a few studies have investigated the ability of QPEs derived from real-world CML networks for quantitative hydrology, either for rural (Brauer et al., 2016; Cazzaniga et al., 2020; Smiatek et al., 2017) or urban catchments (Disch et al., 2019; Stránský et al., 2018). The studies from urban environments have

suggested that CML QPEs could be conveniently used in combination with other rainfall data, e.g. to disaggregate cumulative rainfall measurements from point rain gauges, if available in high temporal resolutions. However, many questions regarding applications of CML QPEs, especially correction of their systematic errors, remain open.

2.3 CML QPE errors

Most errors in CML QPEs could be linked with the following two main uncertainty types:

- Instrumental uncertainties associated with the individual microwave link measurements;
- Spatial uncertainties related to the CML spatial representativeness and the way the spatial information is processed (e.g. for rainfall field reconstruction).

2.3.1 Instrumental errors

QPEs are more prone to be biased for CMLs with shorter path lengths and lower frequencies (Leijnse et al., 2008). These CMLs are less sensitive to rainfall, and raindrop-induced attenuation A_r thus constitutes only a relatively small part of the observed $TRSL$ (Eq. 2.2). In other words, QPEs from these CMLs are more sensitive to errors in the process of A_r estimation. Let us illustrate this problem with a brief didactic example.

For a 1-km-long CML working at a frequency of 32 GHz, the raindrop attenuation A_r caused by the rainfall of 20 mm/h is about 4 dB. However, for a CML with the same frequency and a path length of 4 km, A_r equals roughly 15 dB. If A_r is overestimated by 1 dB, a common value due to the instrumental uncertainties, the derived precipitation rate is overestimated by approximately 30% for the 1-km CML, and by 10% for the 4-km one (see Fig. 2.1). This becomes worse if the rainfall intensity is only 3 mm/h, because the relative errors in CML QPEs rise to 175% and 40% for the 1-km and 4-km CMLs respectively. Furthermore, for low rainfall rates, the derived rainfall is very sensitive to the CML frequency, and thus higher errors are associated with lower frequencies.

The following main potential instrumental error sources were identified by Leijnse et al. (2010), with the last two being most important for the bias in the estimated rain rates (Chwala & Kunstmann, 2019):

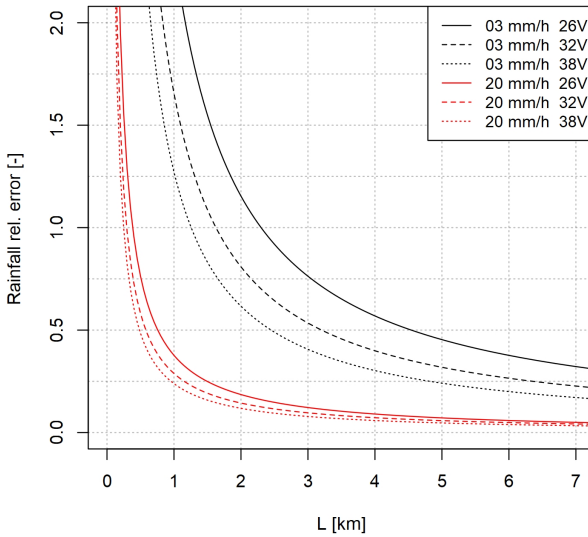


Figure 2.1: The relative error in QPEs from CMLs with vertical polarization in relation to CML path length for two rainfall intensities (3 and 20 mm/h) and three CML frequencies (26, 32, 38 GHz) as caused by an error of 1 dB in the estimate of A_r due to instrumental uncertainties.

- Too coarse temporal sampling
- Quantization of $TRSL$ values
 - Commonly used quantization levels of the records of transmitted and received radio signal power, used to calculate $TRSL$, are 1 dB and 0.33 dB respectively
- Wet antenna attenuation
 - Details in 2.3.1
- Uncertainty of the baseline level B
 - B can be identified from dry-weather attenuation levels

■ **Wet antenna attenuation**

WAA is, in contrast to A_r and B , independent of CML path length. Previous studies (Leijnse et al., 2008; Overeem et al., 2011) also suggest that it is relatively insensitive to CML frequency at bands suitable for rainfall retrieval (20–40 GHz). However, the complexity of the antenna wetting process is a major challenge to reliable WAA estimation.

Antenna wetting is influenced not only by rainfall, but by other atmospheric conditions (e.g. wind, temperature, humidity or solar radiation) and also

antenna hardware properties (e.g. antenna radome material or coating; van Leth et al., 2018). Thus, to date, there is no unified approach to estimate WAA and reported WAA models are often based on different assumptions and result in considerably different estimates. For example, drying times of up to several hours have been reported (Schleiss et al., 2013), whereas other studies have not considered any wetting or drying dynamics at all, relating WAA only to rainfall intensity (Valtr et al., 2019; Kharadly & Ross, 2001).

It has also been suggested to estimate WAA based on water quantity and distribution (droplets, rivulets, water film) on antenna radomes (Leijnse et al., 2008; Mancini et al., 2019). Recently, it has been shown that WAA can be estimated using antenna reflectivity acting as a proxy variable for water film thickness (Moroder et al., 2019). However, applying this model is significantly limited by the unavailability of the required antenna reflectivity measurements.

Since having a globally valid WAA model only depending on known CML characteristics such as frequency does not seem possible, optimal WAA models should ideally be determined for each individual CML. This is especially true for models whose parameters depend on CML path length (e.g. Kharadly & Ross, 2001). However, optimal WAA model identification (e.g. for calibration purposes) on the level of individual CMLs is challenging, especially for real-world application with networks consisting of a high number of CMLs. As noted by (Ostrometzky et al., 2018), maintenance of dedicated equipment for the retrieval of the needed reference rainfall observations is impractical for such networks.

Due to all the above issues, application-focused studies with city or regional-scale CML networks have often not applied any WAA correction at all (Chwala et al., 2012; Smiatek et al., 2017) or have used only a simple constant offset model (Overeem et al., 2011; Roversi et al., 2020; Fencl et al., 2020). Although the latter approach may be a reasonable choice when only 15-min TRSL maxima and minima are available (Chwala & Kunstmann, 2019), it can introduce considerable bias in the resulting CML QPEs (Fencl et al., 2019).

Fencl et al. (2017) proposed adjusting the CML QPEs to measurements from traditional rain gauges if these are available in the vicinity of CMLs. Such adjusted high-resolution CML QPEs can outperform rainfall data derived only from the gauges used for adjusting (Fencl et al., 2017). The adjustment, however, leads to underestimation of peak rainfalls, and it is not clear how this will affect hydrological modelling, since it has never been investigated experimentally on an extensive data set.

Calibration to reference (rainfall) data seems to be a reasonable way to achieve reliable WAA models. However, reference rainfall retrieval approaches employed in research studies which include intensive monitoring campaigns

(e.g. Schleiss et al., 2013; van Leth et al., 2018) are impractical for high numbers of CMLs due to the costs associated with the dedicated equipment needed. Alternatively, already existing rain gauge networks or high-resolution weather radars might be used to calibrate the WAA models. However, as discussed above, such rainfall data sources are often not readily available to urban hydrologists. Moreover, the potential usefulness of CML QPEs increases with the decreasing availability of other rainfall (or other reference) data. Thus, it would come handy if WAA models could be calibrated using better available data and tools, such as low resolution rainfall measurements or stormwater discharge observations in combination with a rainfall-runoff model.

■ 2.3.2 Spatial errors

(The spatial uncertainties related to interpolation are low (?) compared to individual link instrumental errors)

A lot of work was done on rainfall fields for large areas (e.g. countries). However, spatial rainfall field reconstruction from the path-integrated CML data (D'Amico et al., 2016; Goldshtain et al., 2009; Haese et al., 2017) remains unappealing for many potential CML QPE applications, e.g. due to the low hydrological model complexity or small catchment area. For such tasks where areal rainfall estimates are satisfying and several CMLs are at hand, the influence of different CML topologies on the estimated areal rainfall (Fencl et al., 2015) and simulated runoffs (Pastorek et al., 2019b) has been investigated. These studies have concluded that

the position of CMLs in respect to the small urban catchment affects their ability to capture rainfall-runoff dynamics, such as the onset of a runoff event, timing of the hydrograph rising limb, runoff peak, and recession limb;

CMLs with short paths, which typically correspond well to (sub-)catchment scales are often considerably biased, what compromises their usability for urban hydrology

combining QPEs from all available CMLs can very well capture the rainfall, and it is recommended when no prior information on CML data quality is available.

In addition, Fencl et al. (2015) concluded that a few very precise (i.e. least biased) CMLs will deliver the most accurate areal QPEs. However, they compared the CML QPEs only against reference rain gauge data. Nevertheless, if the QPEs are meant to be used in hydrological applications such as r-r modelling, where the spatial relations of CMLs and a catchment are of

high importance, this problem should be investigated in the rainfall-runoff modelling context.

Moreover, if the bias in QPEs is relatively comparable among the CMLs, it is not clear how to identify optimal subsets of CMLs in such conditions. It remains to be investigated in what other ways such subsets could be identified efficiently. For example, it should be investigated whether the CML spatial relations with the catchment can be used as the only decisive criteria. If this was proved to be efficient, it could considerably improve the value added of CMLs under data scarce conditions. Alternatively, if suitable reference data are available, the CML subsetting could be optimized by calibration to these data

2.4 Rainfall Data Set Evaluation

It is a common approach, applied as well in the studies of Fencl et al. (2015, 2017), to evaluate and benchmark rainfall data time series by a direct comparison with a referential (typically best-casescenario) time series. A chief problem here is the limited representativeness of the referential rainfall data set. If, as reference, we use even high-quality precipitation measurements, e.g. from a relatively dense network of rain gauges, the information about precipitation included in such data can differ significantly from the true incident rainfall over a given area. Furthermore, if we were to evaluate a data set which better describes the ground-truth precipitation than the referential rainfall data, the improvement could not be captured with this approach. This could be very unfortunate especially if we dealt with rainfall data of unknown characteristics.

The same issue can arise also in studies where various rainfall data sets are evaluated primarily for purposes of hydrological modelling, such as the study of Ochoa-Rodriguez et al. (2015) on the impact of spatial and temporal resolution of rainfall inputs on urban hydrodynamic modelling. In this study, modelling results obtained using various rainfall data sets were evaluated using as reference the modelling results associated to the finest resolution rainfall estimates. Furthermore, in this type of studies, it is unclear whether the best-quality rainfall data always (e.g. even when the model used was calibrated using another rainfall data set) lead to the best model performance.

River (resp. drainage system) discharges, especially in urban areas, closely reflect transformed rainfall aggregated for a whole given catchment. Furthermore, they are typically measurable more reliably than the true incident precipitation over the given area. Many questions related to the representativeness of the referential data could disappear if such runoff measurements were employed when evaluating various rainfall data sets. This approach was

2. Theory

previously applied both in natural (e.g. Obled et al., 1994; Segond et al., 2007) and urban (Berne et al., 2004) catchments.

The study of Berne et al. (2004) investigated spatiotemporal rainfall-runoff dynamics in Mediterranean urban areas, among others, from the point of view of rain measurements integrated to various temporal resolutions. The relation between the precipitation and runoff was quantified only using the lag time, which is “the time difference between the gravity centre of the mean rainfall over the catchment on one hand and the gravity centre of the generated hydrograph on the other hand”.

However, when evaluating rainfall data sets for the purposes of hydrological modelling, using a rainfall-runoff model to evaluate rainfall data of interest is a common approach (Goormans and Willems, 2013, Wang et al., 2015). Moreover, stormwater runoff can be considered as a proxy variable of catchment areal rainfall, which can be especially useful in the case of convective precipitation, when the true incident rainfall over a given area is often difficult to estimate using traditional reference rainfall measurements. This was done also in the studies of Obled et al. (1994) and Segond et al. (2007), even though they investigated natural catchments. Focusing specifically on urban stormwater modelling, Kleidorfer et al. (2009) studied the impact of (artificially created) imperfections in rainfall data on urban drainage model parameters. In this study, and as well in a similar study of Dotto et al. (2014), it was found that systematic rainfall errors can have a significant impact on model parameters, resp. model outputs.

By employing rainfall-runoff modelling, additional uncertainties are being introduced into the process of rainfall data evaluation. It has been argued that ignoring the uncertainty, particularly related to input data, compromises (not only) hydrological modelling (Beven, 2006; Kavetski et al., 2006), or similarly, that quantification of the uncertainty associated with the models in urban stormwater modelling is a must (Dotto et al., 2012). However, quantifying the effect of all principal uncertainty sources (or, specifically, the effect of uncertainty related to rainfall data) on rainfall-runoff modelling results is a complex and challenging task. Therefore, though conceptually desirable, it is rarely practiced (Dotto et al., 2012). Researchers have often been avoiding it by trying to maximize the reliability of modelling results, e.g. by using data measured over a long period of time (e.g. Segond et al., 2007), or by employing “verified and operational models” (Ochoa-Rodriguez et al., 2015).

Whether the uncertainty analysis is employed or not, there are various methods to evaluate the performance of a rainfall-runoff model. The primary output of a rainfall-runoff model is a time series of simulated discharges at a given location. Such a time series is well suited to being evaluated visually, creating a hydrograph. However, for numerical evaluation, it is preferable to summarize the performance in a single metric (or a small number of metrics).

Many metrics often represent only a specific part (e.g. maximal discharge) or only a certain aspect (e.g. temporal precision, total volume discharged) of the hydrograph. If multiple rainfall-runoff events or even various catchments are to be compared, it is preferable to use standardized dimensionless criteria, e.g. the relative error of maximal discharges. Alternatively, there are metrics which take into account the whole time series and are often applied when trying to summarize the overall model performance, such as the mean squared error (MSE) or Nash-Sutcliffe efficiency (NSE). These two metrics are used very commonly in hydrological modelling although it has been shown that there are systematic problems inherent with their usage (Gupta et al., 2009).

2.5 Prediction uncertainty quantification in hydrology

Deletic et al. (2012) reviewed studies investigating uncertainty in urban hydrological modelling and identified the following key uncertainty sources:

1. Model input (measured input data and parameters) uncertainties;
2. Calibration (calibration data measuring, availability, and choices; calibration algorithms and objective functions used in the calibration process) uncertainties;
3. Model structure (conceptualisation errors, equations and numerical methods) uncertainties.

Many published urban drainage modelling studies have dealt with uncertainties associated with model parameters, often producing parameter probability distributions and estimating confidence intervals around the model's outputs (e.g. Thorndahl et al., 2008; Dotto et al., 2012). However, Deletic et al. (2012) recognized that the uncertainty sources are highly interlinked, suggesting that assessing the impact of a single source is not going to be adequate and that simultaneous propagation of key sources of uncertainties is required.

Dotto et al. (2012) observed that a common approach when trying to estimate the total uncertainty (related to parameters and all other sources) is adding a Gaussian error term to the model predictions. This approach is based on the assumption that the residuals between the measured and modelled values are normally distributed (i.e. only due to white measurement noise). However, the deviations of model outputs from observed data are usually considerably larger than random observation errors, typically due to a simplified description of the system by the deterministic model and due to input data imperfections (Reichert & Schuwirth, 2012). When ignored, such systematic deviations

2. Theory

can lead to unrealistic (usually too narrow) uncertainty bounds of model parameters and model predictions (Reichert & Schuwirth, 2012).

Systematic deviations of model predictions from observed data, or model bias, can be addressed by increasing the complexity of the model to reduce bias or by trying to find a statistical description of the bias in model outputs. Reichert & Schuwirth (2012) adapted a statistical technique of Kennedy & O'Hagan (2001), accounting for bias in model outputs, for purposes of environmental modelling and extended it with a framework enabling for multiobjective model calibration. Del Giudice et al. (2013) later applied this technique to urban drainage modelling while proposing various formulations of the stochastic process representing the model bias (more in section 2.6). Their results showed that runoff simulations are much more reliable when bias is accounted for than when it is neglected.

While approaches based on explicit model bias consideration can improve the reliability of hydrological predictions, they only provide limited information about the causes of model bias and, therefore, do not help much to distinguish imperfections in input rainfall data from model structural errors (Del Giudice et al., 2013). A conceptually more satisfying approach is to make the input uncertain and to propagate it through the model. This can be done by using so-called rainfall multipliers (Kavetski et al., 2006; Vrugt et al., 2008). These random variables multiply observed rainfall rates (1 multiplier per event) before feeding it into the model. They are estimated together with other model parameters and allow to quantify the rainfall-related uncertainty directly in input data. Sikorska et al. (2012) combined a stochastic error model with rainfall multipliers to separate the effect of uncertainty in the rainfall data from other errors sources. However, the rainfall multiplier approach fails when the observed precipitation has a different temporal pattern from the true one or if the true nonzero rainfall is not detected (Del Giudice et al., 2016).

To overcome the above problem, Del Giudice et al. (2016) introduced a method where the average precipitation over a given catchment is formulated as a stochastic process, parameters of which are inferred together with other model parameters during calibration. They showed that, even when starting with inaccurate precipitation data, this approach can accurately reconstruct the whole-catchment precipitation and reliably quantify the related uncertainty. However, their results suggested that even a simpler approach (e.g. Del Giudice et al., 2013) can lead to similar model parameters and prediction intervals. Therefore, if precipitation reconstructing is not of major interest, the novel approach is not appealing, given its high computational requirements.

2.5.1 Performance assessment

When dealing with interval predictions, it is common to evaluate two aspects of the predictive performance – its precision and accuracy. The prediction precision can be quantified by the width of the determined confidence interval, referred to also as interval sharpness (e.g. Breinholz et al., 2012). The prediction accuracy can be understood as the position of observed value(s) in relation to the confidence bound(s). Time series predictions such as hydrographs can also be assessed in this manner, e.g. by calculating the prediction reliability, i.e. the share of observed data points within the predicted bounds, and the “average bandwidth” – the interval widths averaged over the entire prediction period (Del Giudice et al., 2013).

Gneiting & Raftery (2007) proposed a metric which combines the two above aspects – the interval score S_α . For a single interval prediction at a confidence level $1 - \alpha$ (determined by the prediction quantiles at levels $\frac{\alpha}{2}$ and $1 - \frac{\alpha}{2}$), the interval score

$$S_\alpha(l, u, x) = (u - l) + \frac{2}{\alpha}(l - x)\mathbb{1}\{x < l\} + \frac{2}{\alpha}(x - u)\mathbb{1}\{x > u\}, \quad (2.3)$$

where l and u stand for lower and upper interval bounds. This metric is supposed to allow for intuitive comprehension as “the forecaster is rewarded for narrow prediction intervals and incurs a penalty, the size of which depends on α , if the observation misses the interval” (Gneiting & Raftery, 2007).

For time series prediction, the idea of S_α can be extended and the mean interval scores (MIS) for a given period can be quantified. Bourgin et al. (2015) further developed the concept and, “to ease comparison between catchments and evaluate the skill of the prediction bounds”, proposed to benchmark the prediction confidence bounds by MIS for reference bounds (MIS_{ref}) obtained e.g. from long term climatological data. The mean interval skill score $MISS$ would be computed as

$$MISS = 1 - (MIS/MIS_{ref}), \quad (2.4)$$

high values of which indicate greater prediction skill, with positive scores indicating that evaluated predictions are more skillful than the reference.

2.6 Explicit statistical consideration of model bias

Herein we describe the framework of Kennedy & O’Hagan (2001) as formulated by Reichert & Schuwirth (2012) and first used in the context of urban hydrology by Del Giudice et al. (2013). The basic principle of the method is extension of a deterministic (e.g. rainfall-runoff) model by a stochastic error

2. Theory

model. However, a commonly used error model considering only independent and identically distributed (i.i.d.) errors is adjusted to explicitly account for the systematic model errors (bias) of the deterministic model, acknowledging the fact that simulators cannot describe the true behavior of a system (Del Giudice et al., 2013). Using this approach, the extended model can be formulated using the equation

$$Y_o(x, \theta, \psi) = y_M(x, \theta) + B(\psi) + E(\psi) \quad (2.5)$$

where variables in capitals represent random variables and those in lowercase are deterministic functions. Y_o represents the observed system output, y_M stands for the deterministic model output. To better fulfill the underlying statistical assumptions and thus obtain more reliable predictions, a transformation (details in 2.6.1) should be applied on both Y_o and y_M (Del Giudice et al., 2013). Next, B and E , respectively, stand for the bias and measurement noise in the system output. Precipitation as the external driving force is represented by x , whereas θ and ψ respectively represent the deterministic and error model parameters.

The measurement noise of the system response E is sampled from a multivariate normal distribution with mean 0 and a diagonal covariance matrix

$$\Sigma_E = \sigma_E^2 \mathbb{1} \quad (2.6)$$

Del Giudice et al. (2013) investigated various formulations of the model bias B and presented a structured approach to select the optimal bias description for a given case study. In general, it is an autoregressive term which can be dependent on the input (rainfall) or/and output (runoff) of the system. For more details, see Del Giudice et al. (2013).

By combining the deterministic hydrological and the stochastic error models, we can quantify the probability that the observed runoffs can be explained by given predicted runoffs and error model. This can be formally expressed by a likelihood function describing the joint probability density $f(Y_o|\theta, \psi, x)$ of observed system response Y_o for given θ , ψ , and x . It can be written as

$$f(Y_o|\theta, \psi, x) = \frac{(2\pi)^{-\frac{n}{2}}}{\sqrt{\det(\Sigma(\theta, \psi, x))}} \cdot \exp\left(-\frac{1}{2}[\tilde{Y}_o - \tilde{y}_M(\theta, \psi, x)^T \Sigma(\theta, \psi, x)^{-1}] [\tilde{Y}_o - \tilde{y}_M(\theta, \psi, x)] \prod_{i=1}^n \frac{dg}{dy}(Y_{o,i}, \psi)\right), \quad (2.7)$$

where n is the number of observations (i.e. the dimension of Y_o and y_M) and $\Sigma(\theta, \psi, x)$ stands for a covariance matrix of the residuals transformed by a function $g()$. Similarly, $\tilde{y}_M = g(y_M)$.

To achieve accurate rainfall-runoff predictions and reliable quantification of their uncertainty, the extended model should be calibrated. In theory, this

could be done by optimizing the likelihood function as the objective function. However, there is “a severe identifiability problem” between the deterministic model y_M and bias B “as the two components cannot be observed separately” (Reichert & Schuwirth, 2012). By implementing the Bayesian approach, i.e. combining the likelihood with prior knowledge (belief) about the extended model, we can specify that we are seeking for the smallest bias possible when calibrating the model. Although somewhat subjective choices regarding the amount of bias acceptable are required, this approach at least makes them transparent (Reichert & Schuwirth, 2012).

Performing the uncertainty analysis in the above described manner requires to follow these steps (Del Giudice et al., 2013):

1. Definition of marginal distributions of the prior joint probability distribution of the both the deterministic rainfall-runoff model parameters θ and the stochastic error model parameters ψ .
 - Del Giudice et al. (2013) suggest that completely uninformative prior distributions should not be used for neither θ nor ψ parameters. Furthermore, it is “important that the prior of the bias reflects the desire to avoid model inadequacy as much as possible ... to reduce the identifiability problem between the deterministic model and the bias”.
2. Bayesian inference of the posterior parameter distribution.
 - The joint probability density, a product of the prior $f(\theta, \psi)$ and the likelihood function $f(Y_o|\theta, \psi, x)$, gets conditioned on the observed discharge data, using the Bayes’ theorem

$$f(\theta, \psi|Y_o, x) = \frac{f(\theta, \psi) f(Y_o|\theta, \psi, x)}{\int \int f(\theta', \psi') f(Y_o|\theta', \psi', x) d\theta' d\psi'} . \quad (2.8)$$

Solving this problem analytically would include dealing with multidimensional integrals. This can be avoided by employing a numerical method such as Markov Chain Monte Carlo (MCMC) to approximate properties of the posterior distribution.

- Before the inference, a transformation $g()$ should be applied on simulation results and output data to account for the variance increasing with discharge and to reduce the heteroscedascity of residuals (Del Giudice et al., 2013). Details in 2.6.1.
- 3. Probabilistic predictions for the data set used for calibration
 - For details on probabilistic predictions for multivariate normal distributions related to the random variables of this type, Del Giudice et al. (2013) recommend to consult Kendall et al. (1994) or Kollo & von Rosen (2006).

4. Probabilistic predictions for unseen temporal points.

- It is possible to proceed analogically as above. However, Del Giudice et al. (2013) suggest to take advantage of using bias formulated as an Ornstein–Uhlenbeck process and to “draw a realization for the entire period by iteratively drawing the realization for the next time step at time t_j from that of a previous time step at time t_{j-1} from a normal distribution”. In both cases, nevertheless, it is necessary to draw and evaluate a large sample from the posterior parameter joint distribution.

5. Verification of the statistical assumptions

- In many similar cases, it is usual to confirm the statistical assumptions of the error model by residual analysis (Reichert & Schuwirth, 2012). However, Bayesian approach implemented in this method allows us to test only the observation error E , which is the only purely frequentist term. However, since these errors are likely to constitute only a small portion of the residuals of the deterministic simulator, the informative value of this analysis might be limited.

2.6.1 Output transformation

Because of the statistical assumptions of homoscedasticity and normality of calibration residuals, a transformation $g()$ should be applied on simulation and observed output data (i.e., in our case, runoff discharges). It is a common way in hydrological modelling how to account for increasing variance with increasing discharge and thus reduce the residual heteroscedascity. Moreover, it is expected to reduce the proportion of negative flow predictions by making error distributions asymmetric (Del Giudice et al., 2013).

According to Del Giudice et al. (2013), two most promising variance stabilization techniques for urban drainage applications are the Box–Cox (Box & Cox, 1964) and the log-sinh (Wang et al., 2012) transformation. The Box-Cox transformation has been used more often in hydrological studies than the log-sinh alternative, primarily due to the date of its first introduction. The two-parameter Box–Cox transformation can be written as

$$g(y) = \begin{cases} \log(y + \lambda_2), & \text{if } \lambda_1 = 0 \\ \frac{(y+\lambda_2)^{\lambda_1}-1}{\lambda_1}, & \text{otherwise} \end{cases} \quad (2.9)$$

and holds for $y > -\lambda_2$. The one-parameter version would need only λ_1 while keeping $\lambda_2 = 0$. Del Giudice et al. (2013) used the one-parameter version of the transformation with the parameter value $\lambda_1 = 0.35$, which had already been proven to perform satisfactorily in the past (e.g. Honti et al., 2013; Wang et al., 2012).

The log-sinh transformation was introduced for hydrological purposes only recently by Wang et al. (2012). Del Giudice et al. (2013) proposed its modification which would result in a “reparameterised form with parameters that have a more intuitive meaning”. The formula would be

$$g(y) = \beta \log\left(\sinh\left(\frac{\alpha + y}{\beta}\right)\right), \quad (2.10)$$

where α and β represent lower and upper reference outputs. This means that “ α controls how the relative error increases for low flows” and “for outputs larger than β , the absolute error gradually stops increasing” (Del Giudice et al., 2013).

Chapter 3

Material

This chapter is about the material used in the studies presented in the following chapters.

The data used originate from an experimental urban catchment (Fig. 3.1) with an area of 1.3 km² which lies in Prague-Letňany, Czech Republic, and is drained by a separate stormwater drainage system. Approximately 35% of the catchment area is covered by impervious surfaces. The catchment is slightly inclined to the north, with the altitude gradually declining from roughly 280 to 250 m above sea level (Baltic 1957 height, EPSG:8357). The lag time between rainfall peak and runoff peak observed at the outlet from the catchment's drainage system is approximately 20 minutes.

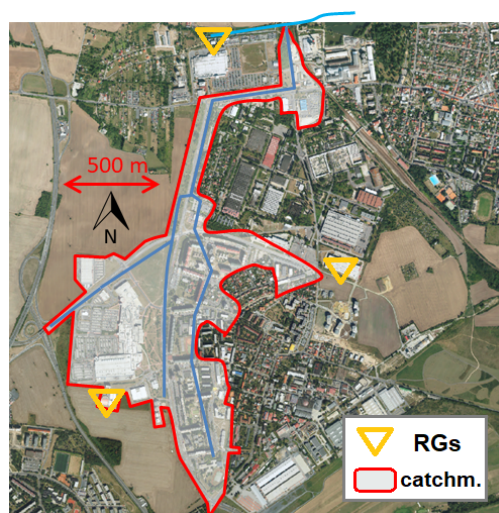


Figure 3.1: Aerial view of the urban catchment studied with the main sewers and receiving water body as well as the position of the local rain gauges (RGs).

3.1 Data retrieval and availability

We monitored 19 CMLs (Table 3.1; Fig. 3.2) and several rain gauges located in the catchment's surroundings (Figs. 3.1 and 3.2) over the period between July 2014 and October 2016, excluding the winter months (December–March) as CML signal attenuation by frozen precipitation, occurring in winter periods, is considerably different than that of liquid precipitation. Moreover, our monitoring setup is designed for periods with liquid precipitation only, as the rain gauges are not heated.

The CMLs (Mini-Link, Ericsson) broadcast at frequencies from 25 to 39 GHz, their lengths are between 611 and 5795 m, and they are operated by a major telecommunication service provider. Long CMLs extend out of the catchment for several kilometers. Signal-level data from CMLs, featuring a common quantization of 1 dB and 0.33 dB for the transmitted and received signal power, were retrieved at a 10-s resolution with a custom-made logging script (Fencl et al., 2015) and then aggregated to a 1-min resolution.

All tipping bucket rain gauges in the area (Figs. 3.1 and 3.2) were produced by the same manufacturer (MR3, Meteoservis) and feature the same characteristics: A funnel area of 500 cm², a bucket volume of 5 ml, and a single tip corresponding to 0.1 mm of rainfall. They are all dynamically calibrated (Humphrey et al., 1997) every year and the rainfall data they provide is stored at a 1-min resolution. However, the rain gauges make part of two different networks. Those located one km or more outside of the catchment (Fig. 3.2) are operated and maintained by the municipal sewer authority as a part of their long-term monitoring network with a density of one gauge per 20–25 km². These gauges are further referred to as “municipal”. In contrast, rain gauges temporarily installed at three locations around the catchment boundaries (Fig. 3.1) for research purposes are referred to as “local”.

In addition, we measured discharges at the stormwater drainage system outlet (Fig. 3.2) using an area-velocity flow meter (Triton, ADS). The flow meter was calibrated in a standard way using stream gaging and the velocity-area method employing an electromagnetic velocity probe. The temporal resolution of the discharge measurements is 2 min for wet periods and 10 min for dry periods. Observed discharge values range from approximately 2 to 2000 l/s.

During the observation period, we observed more than 100 relevant rainfall events with depths exceeding 2 mm. However, due to outages in data from the monitoring devices, it was possible to analyze data from only a considerably lower number of events. The exact number differs for each study presented due to using data from various sets of devices, the availability of the data at a given time, or differences in event definition. Details on rainfall characteristics

ID	FreqA [GHz]	FreqB [GHz]	Polarization	Length [m]
1	31.82	32.63	V	611
2	32.63	NA	H	645
3	NA	32.63	V	816
4	38.88	38.60	V	911
5	24.55	25.56	V	1022
6	37.62	37.62	V	1086
7	37.62	38.88	V	1396
8	37.62	38.88	V	1584
9	31.82	32.63	V	1858
10	24.55	25.56	H	1953
11	38.88	NA	V	1979
12	31.82	32.63	V	2611
13	24.55	25.56	V	2957
14	24.55	25.56	V	3000
15	24.55	25.56	V	3195
16	24.55	25.56	V	3432
17	25.56	24.55	V	4253
18	24.55	25.56	V	4523
19	24.55	25.56	V	5795

Table 3.1: Characteristics of the CMLs observed. FreqA and FreqB are CML frequencies for the two directions. The NA values indicate that records are not available. Polarization (Vertical/Horizontal) is the same for both directions.

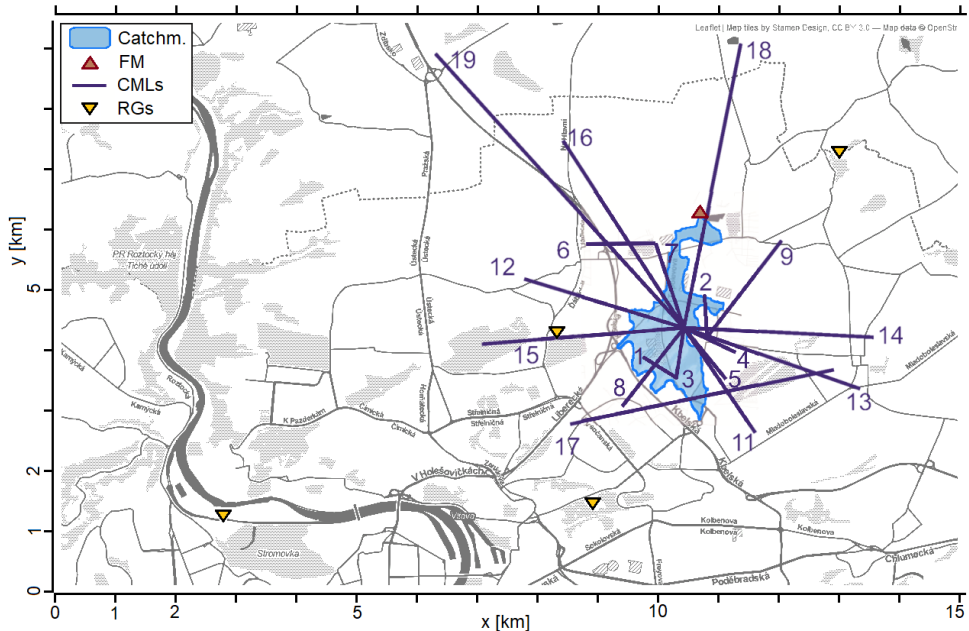


Figure 3.2: Spatial relations of the catchment, the flowmeter (FM), the CMLs (with IDs denoted), and the monitored municipal rain gauges (RGs).

for events as used in the study presented in chapter 5 (see ??) are provided in Appendix ???.

An overview of CML data availability during the monitoring period is shown in Appendix ????. Data from each CML were available, on average, during 80% of the events. Six CMLs had data availability higher than 95% and only two of them lower than 50%. Due to long-term outages, data from CMLs #1, #2, and #10 were analyzed only in the study presented in chapter 4, which investigated only a shorter period during which the data from these CMLs were available.

3.2 Rainfall-runoff model and its reliability

To simulate discharges at the drainage system outlet, an EPA-SWMM model is used which was constructed using detailed information about the catchment (e.g. the ratio of impervious areas for individual subcatchments) and the drainage system (e.g. pipe materials and diameters) provided by the municipal water management authority. The process of runoff generation is formulated empirically and separately for each model subcatchment (195 in total) using the respective surface-depression-storage-depth parameters. The subsequent runoff itself is modeled as one-dimensional flow expressed by Saint-Venant equations. These are numerically solved in the approximated form of a kinematic wave for surface runoff and in the full form of a dynamic wave for the following runoff in the stormwater drainage network. The model was calibrated using an independent data set, i.e. measurements obtained from the three local rain gauges (Fig. 3.1) before the above specified observation period (Pastorek, 2014).

In the cases of all rainfall data sets studied, except for the local rain gauges, the rainfall model input is always implemented as areal rainfall in the model, meaning that rainfall intensity in a given time step has a constant value over all model subcatchments. For the local rain gauges, the catchment is divided into three Thiessen polygons, corresponding to the local gauges at three locations. This means that every subcatchment is assigned the same rainfall intensity as measured at the closest local rain gauge.

The reliability of model predictions was tested using rainfall data from the three local rain gauges, i.e. the same devices that were used for the model calibration. This verification was performed for 59 rainfall-runoff events (see ??) from the observed period between July 2014 and October 2016. Hydrographs for all analyzed events are provided in Appendix ????. Results of this verification are summarized in Fig. 3.3. These results suggest that the model predicts very realistic rainfall runoff. First, on average 78% of simulated discharges fall within the 95% confidence bands of observed runoff

3.2. Rainfall-runoff model and its reliability

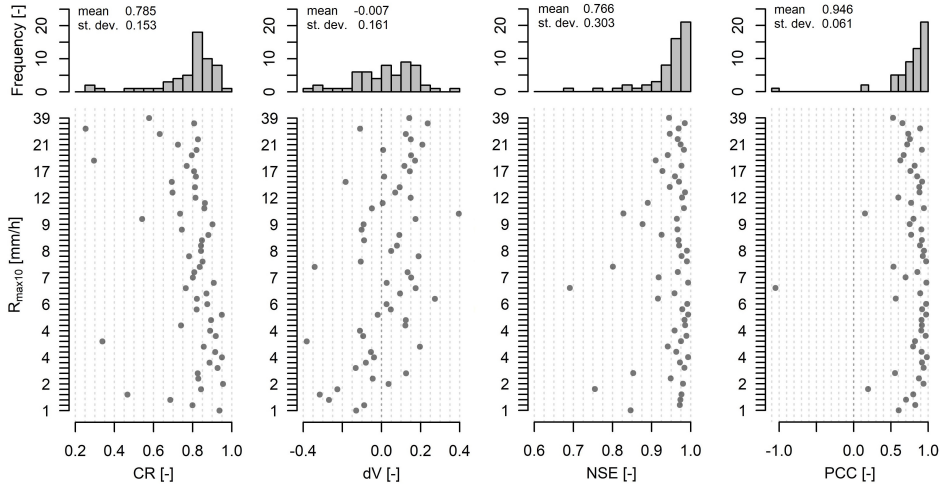


Figure 3.3: Results of the rainfall-runoff model verification. Top: Histograms of the statistics for all evaluated events. Bottom: Scatter plots showing the statistics for single events with respect to the maximal 10-minute rainfall intensity ($R_{max,10}$) observed by the local rain gauges during these events.

defined by 2.5% and 97.5% quantiles of observation errors (see section 5.2.4), i.e. the mean containing ratio $CR [-]$ is 0.78, and its st. dev. is 0.15. Second, the relative error in volume on average is only -0.7%, and modelled discharge shows a 0.95 Pearson's correlation coefficient in relation to the observed values. The Nash–Sutcliffe efficiency is also high (mean 0.77 and st. dev. 0.3). The model performs less satisfactorily in terms of predicting peak flows during heavy rainfalls, they are often substantially overestimated (on average by 40%). This is probably related to errors associated with the rainfall measurement or strong assumptions regarding rainfall spatial variability over the catchment area. For some of the heaviest rainfalls, peak flows are overestimated by more than 100%, which is probably also due to the model structural deficiencies, e.g. unmodelled overland flows during extreme events. In summary, the rainfall-runoff model performs very well except for extreme events.

Chapter 4

On the value of CML QPEs for urban rainfall-runoff modelling: The pilot study

Rainfall-runoff modelling in urban catchments requires reliable rainfall data with high temporal and spatial resolution. Such data are often not available and, thus, unmeasured spatial rainfall variability is an important source of uncertainty in urban rainfall-runoff modelling. Recently, commercial microwave links (CMLs), an extensively used solution in telecommunication networks, have been introduced as a new potential source of rainfall data with the necessary resolution. We compare this novel rainfall data source with more conventional sources from point rain gauges based on a comparison of measured runoffs with rainfall-runoff modelling results of a small urbanized catchment obtained using the researched rainfall data sets. We employ a method based on Bayesian inference to calibrate our rainfall-runoff model and to estimate the uncertainty of modelling outputs. Results of the performed analyses show that CML rainfall data, when a suitable adjustment is applied (e.g. using information from nearby rain gauges), allow for better detection of dynamics of precipitation and subsequent runoff than data from point rain gauges alone, especially in the case of heavy rainfalls which are highly variable in space and time. Therefore, microwave links represent a relevant rainfall data source, which can conveniently complement existing rainfall monitoring networks.

The bulk of this chapter was originally published in Pastorek et al. (2017, 2018).

4.1 Introduction

Reliable rainfall data are crucial when performing urban rainfall-runoff modelling. Nevertheless, high spatial variability of rainfall during convective

events negatively affects the representativeness of point precipitation measurements from rain gauges. This could be avoided by employing commercial microwave links (CMLs), which allow for indirect path-averaged precipitation detection and are typically very dense in urban areas. However, to date, only a few studies have investigated the ability of quantitative precipitation estimates (QPEs) from CMLs for quantitative hydrology.

Smiatek et al. (2017) investigated the potential of QPEs from CMLs for streamflow prediction in an orographically complex mountainous region. In urban settings, Fencl et al. (2013) assessed the potential of CMLs to capture spatiotemporal rainfall dynamics and thus improve urban rainfall-runoff modelling, however, using only virtual rainfall fields. In a similar analysis, Fencl et al. (2015) evaluated QPEs derived from real-world CML data, however, without using these for hydrological modelling. Thus, to the best of our knowledge, no research has been presented yet in relevant literature where real-world CML QPEs would be applied for urban rainfall-runoff modelling.

In this study, we target the above research gap and analyze whether QPEs obtained from CMLs can be regarded as a viable alternative for rainfall data in the field of urban rainfall-runoff modelling. As CML QPEs are often highly biased, what limits their usability for practical purposes, we analyze CML QPEs derived using both a standard approach and a recently proposed (Fencl et al., 2017) novel method for adjusting the QPEs to existing rain gauges.

The CML QPEs, as well as traditional data from rain gauges, are propagated through a calibrated rainfall-runoff model and evaluated against observed discharges. Since additional uncertainties are introduced into the process of rainfall data evaluation by employing the rainfall-runoff modelling, we use a thorough statistical method which allows for a reliable quantification of the runoff prediction uncertainty associated with various rainfall observation layouts.

4.2 Methods

The defined problem is addressed using rainfall and runoff data collected in a small urban catchment in Prague-Letňany, Czech Republic (details in 3) during three months (August – October) of 2014. Precipitation time series from six rainfall observation layouts are propagated through a rainfall-runoff model (3.2) and evaluated against observed runoffs. In order to quantify the associated uncertainties, the hydrological model is operated by means of prediction uncertainty quantification as first used in a similar context by Del Giudice et al. (2013) and introduced in section 2.6.

4.2.1 Rainfall observation layouts

We investigate rainfall data observed during 15 rainfall-runoff events from the summer season of 2014 using the six following observation layouts:

1. Measurements from three local rain gauges

Rainfall data from three local rain gauges installed for research purposes (Fig. 3.1) around the catchment of interest. This data set represents rainfall information observed on site which, however, in the context of the Czech Republic, is available only for short term experimental purposes.

2. Measurements from a single local rain gauge

Rainfall data at a 1-min resolution from the local rain gauge located at the south-west catchment boundary (Fig. 3.1). This data set represents rainfall information observed on site which could be available more commonly than the data above, however typically also only for a limited period of time, e.g. in order to evaluate the effect of (re)construction works in the catchment.

3. Measurements from three municipal rain gauges

Rainfall data from the three municipal rain gauges closest to the catchment (Fig. 3.2). Due to their 1-min resolution, for which correlations are low for the given distances (Villarini et al., 2008), only a single time series, constructed as the mean of the instantaneous R [mm/h] values of the three gauges, is evaluated. This data set represents rainfall data standardly available in long-term perspectives in urbanized areas of the Czech Republic.

4. QPEs from the four CMLs adjusted by the local rain gauge,

Data from the single local rain gauge specified above, aggregated to 15-min time steps, is used to adjust (Fencl et al., 2017) CML QPEs with a 1-min resolution. In particular, wet antenna attenuation (A_{wa} from Eq. 2.2) and α (Eq. 2.1) are adjusted, while keeping $\beta = 1$. Only short CMLs (path length < 1500 m) located close to the catchment center are used (#1, #2, #5, #7; Fig. 3.2; #3 and #4 are excluded due to outages and erratic behavior, respectively). Only a single time series, constructed as the mean of the instantaneous R [mm/h] values of the four CMLs, is evaluated. This rainfall data set showcases application of CML QPEs when traditional

rainfall information is available directly in the catchment area, however, not in a satisfying spatial resolution.

5. QPEs from four CMLs adjusted by the municipal rain gauges

The instantaneous mean of the QPEs from the same four CMLs as above, adjusted in the same way, however, using the mean of the data from the three municipal rain gauges (specified above). This rainfall data set showcases application of CML QPEs in situations when rainfall is not measured directly in the catchment, but there are gauges in the distance of 2–3 km, which, however, provide data in lower temporal resolutions (e.g. 15, 30, or 60 min).

6. Unadjusted QPEs from all CMLs available (Fig. 3.2).

The instantaneous mean of QPEs derived, using a standard approach, from all CMLs available in the area in a given time. A_{wa} is estimated as a constant offset with the value of 2.5 dB, which was determined by comparing the specific raindrop attenuation γ [dB/km] of short and long CMLs. The rainfall intensity R [mm/h] is calculated with parameter values α and β chosen in accordance with ITU Radiocommunication Sector (2005). This data set represents a situation when traditional rainfall information is not available in the catchment's surroundings.

In the cases of all CML data, prior to applying the correction for A_{wa} , baseline B [dB] (Eq. 2.2) is separated in the same manner as in Fencl et al. (2017).

■ 4.2.2 Rainfall-runoff modelling and uncertainty analysis

Rainfall time series retrieved using all the five observation layouts are propagated through a rainfall-runoff model (3.2) and evaluated against discharges observed at the outlet from the local stormwater drainage system. When usig rainfall data from the three local rain gauges, the rainfall input is implemented in the model using three Thiessen polygons. This means that the rainfall intensity above a given model subcatchment is assumed to be the same as measured at the closest gauge. In all other cases, rainfall input is implemented as areal rainfall, meaning that rainfall intensity in a given time step has a constant value over all subcatchments of the model.

In order to acknowledge uncertainties of the rainfall-runoff model predictions, we employ uncertainty analysis framework of Kennedy & O'Hagan (2001) as formulated by Reichert & Schuwirth (2012) and first used in a context

similar to ours by Del Giudice et al. (2013). The basic principle of the method (details in section 2.6) is the extension (Eq. 2.5) of a deterministic (i.e., in our case, rainfall-runoff) model by a stochastic error model which explicitly accounts for systematic model errors, i.e. bias.

Del Giudice et al. (2013) investigated various formulations of the model bias and various transformation functions. Based on their recommendations and our previous analyses (Pastorek, 2016), as transformation $g()$, we use the Box-Cox transformation (Box & Cox, 1964) with parameters $\lambda_1 = 0.45$ and $\lambda_2 = 1$. Moreover, we formulate the bias $B(\psi)$ as an autoregressive stationary random process with a long-term equilibrium value of zero and a constant variance. It is a mean-reverting Ornstein-Uhlenbeck process (Uhlenbeck & Ornstein, 1930), “the discretisation of which would be a first-order autoregressive process with Gaussian independent and identically distributed noise” (Del Giudice et al., 2013). It can be expressed using the following differential equation:

$$dB(t) = -\frac{B(t)}{\tau} dt + \sqrt{\frac{2}{\tau}} \sigma_B dW(t), \quad (4.1)$$

where τ represents the correlation time, σ_B the asymptotic standard deviation of the random fluctuations around the equilibrium, and $dW(t)$ a Wiener process, i.e. standard Brownian motion.

By varying the input rainfall data while keeping the rainfall-runoff model structure unchanged, we are able to trace the associated changes in the prediction uncertainty back to the respective rainfall data. However, to achieve accurate rainfall-runoff predictions and reliable quantification of their uncertainty, the extended model should be calibrated first. Although the deterministic rainfall-runoff model has been calibrated in the past, we optimize its parameters also here, together with the stochastic error model parameters, as we aim to maximize both the discharge prediction accuracy and precision.

Prior distribution definition and model calibration

Since the extended model has to be calibrated in a Bayesian framework, prior probability distribution of the model parameters which are to be calibrated must be first defined. Del Giudice et al. (2013) suggest that completely uninformative prior distributions should not be used for parameters of neither the deterministic rainfall-runoff model (θ) nor the stochastic error model (ψ). Furthermore, it is “important that the prior of the bias reflects the desire to avoid model inadequacy as much as possible”. Considering the chosen bias model, σ_B is unlikely to be higher than the variability of observed discharge, τ should represent the characteristic correlation length of the residuals, and σ_E should mirror the measurement noise of the system output Del Giudice et al. (2013).

In accordance with Del Giudice et al. (2013) (see 2.6), we do not use completely uninformative prior parameter distributions. In contrast, the priors are chosen based on knowledge of the urban catchment and consultations with experts who have already used the method. For all the parameters, marginals of the prior joint distribution are defined (Table 4.1) as truncated normal distributions with four defining parameters - mean (μ), standard deviation (σ), minimum, and maximum. It should be noted that ψ parameters σ_B and σ_E are defined in a transformed space via a transformation $g()$. When θ parameters are concerned, they represent multiplicative (scaling) values of the actual model parameters. This means that when a given parameter, e.g. imp , is set to 1.1, the respective imp values for all 195 subcatchments are multiplied by 1.1.

parameter	abbrev.	μ	σ	min.	max.
Percentage of impervious areas [%]	imp	1	1	0.8	1.2
Width of overland flow path [m]	wid	1	1	0.3	1.7
Manning's N for impervious areas	N_{im}	1	1	0.3	1.7
Surface depression storage for impervious areas [mm]	S_{im}	1	1	0.3	1.7
Percentage of impervious areas with no depression storage [%]	$pc0$	1	1	0.3	1.7
Manning's N for drainage pipes	N_{co}	1	1	0.3	1.7
Correlation time [h]	τ	0.5	0.25	0.01	3
Asymptotic stand. dev. of independent errors [$g(1/s)$]	σ_E	$g(0.5)$	$g(0.25)$	0.01	1.5
Asymptotic stand. dev. of the random fluctuations around the equilibrium [$g(1/s)$]	σ_B	$g(50)$	$g(25)$	0	10 000 000

Table 4.1: Summary of the prior marginal distributions.

Data from five out of the 15 available rainfall-runoff events are used to calibrate the extended model. The calibration itself is performed in two steps. First, we use the generalized simulated annealing function of the GenSA package (Xiang et al., 2013), which was designed to “search for global minimum of a very complex non-linear objective function with a very large number of optima”. Second, we use a numerical Monte Carlo Markov Chain sampler as implemented by Scheidegger (2012) according to the proposal of Vihola (2012). This function first tunes the covariance matrix of the jump distribution to achieve a desired acceptance rate. Next, a non-adaptive Metropolis sampling is employed to draw from the posterior distribution.

4.2.3 Performance assessment

After performing the extended model calibration, data from the ten remaining rainfall-runoff events are used to analyze the model predictions. To evaluate the rainfall-runoff predictions visually, we produce hydrographs for each of the ten events and rainfall data from each of the five observation layouts. We do not evaluate the prediction performance by examining separately the uncertainty intervals for the deterministic rainfall-runoff model output. This is in accordance with Del Giudice et al. (2013), who see this approach as “not conclusive because the field observations are not realisations of the deterministic model but of the model plus the errors”. Instead, we only evaluate the total uncertainty intervals associated with the extended model, i.e. the deterministic and the stochastic model together.

We also employ common summary hydrological metrics such as the total discharged volume during a whole given event or the discharged volume during peak flow period. In particular, we compute relative errors of the total discharged volume dV [-] and of the volume during peak flow dV_{peak} [-] for every single prediction of the extended model. When calculating dV_{peak} , the time step with the maximal discharge observed is identified first and the volume discharged during eight minutes around the time step (four minutes before and four after) is computed afterwards. The difference between the modelled time with the maximal discharge and the observed one dt_{Qmax} [h] is another metric we quantify for every model prediction.

The uncertainty in the above metrics dV , dV_{peak} , and dt_{Qmax} is evaluated by calculating the median and other quantiles for the set of predictions associated with a given rainfall observation layout, which are then graphically presented in boxplots. This is in accordance with Fencl et al. (2013) who also used the relative error of the total discharged volume and interpreted its mean \bar{dV} as the metric’s bias and its standard deviation $sd(dV)$ as its uncertainty. Moreover, the discharge prediction reliability associated with a given observation layout is quantified as the fraction of discharge observations falling into the predicted 90% confidence intervals.

To better interpret the results, we classify the rainfall events as either light or heavy, based on the maximal 10-minute precipitation rate.

4.3 Results

First, we present hydrographs showing observed and modelled discharges for a heavy and a light rainfall event which characterize well typical features of the overall results. Next, a summary of the results for all events classified

as heavy (maximal 10-min rainfall intensity $R_{max,10} > 12 \text{ mm/h}$), as light ($R_{max,10} \leq 12 \text{ mm/h}$), and both categories together is presented in boxplots, with a special attention on the heavy rainfalls.

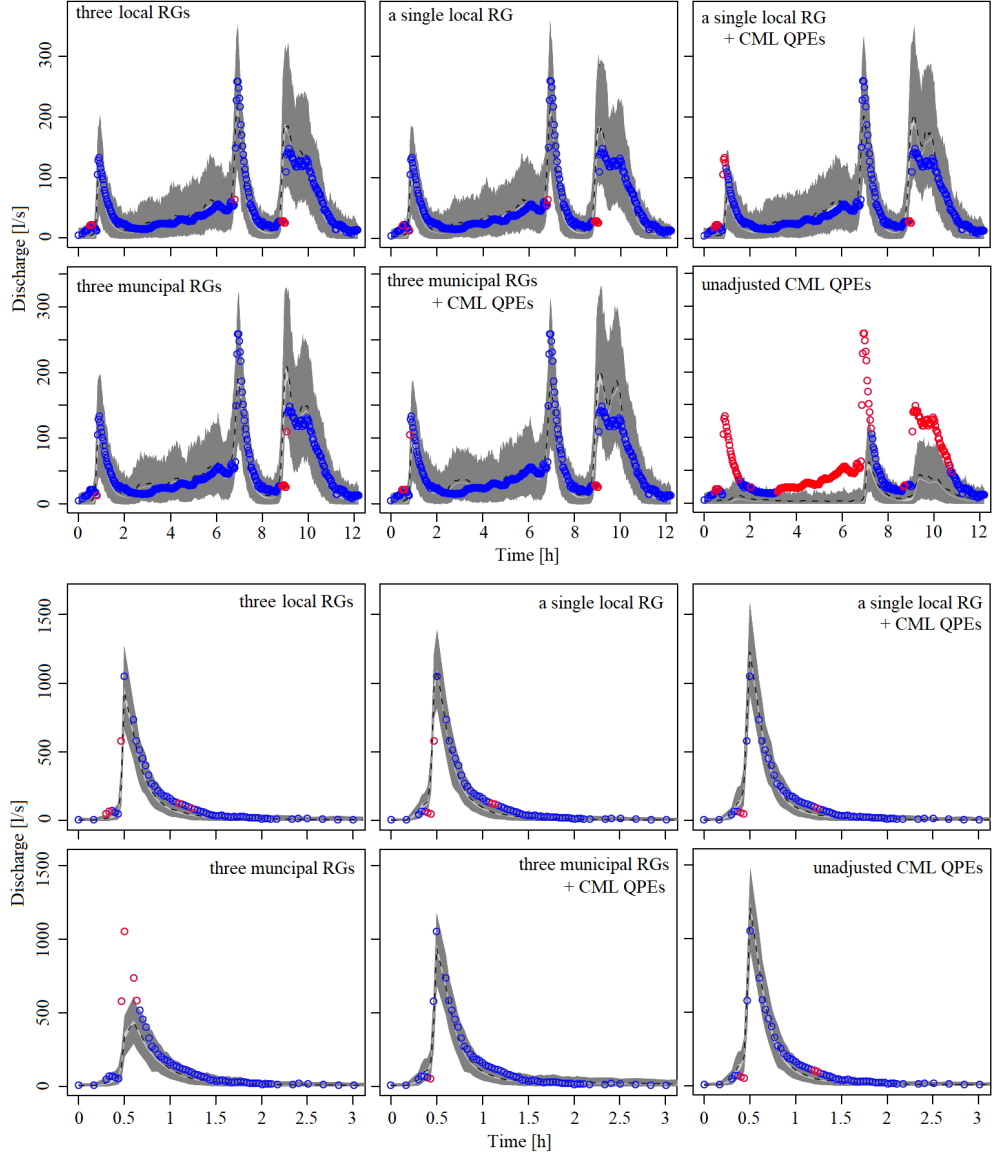


Figure 4.1: Hydrographs associated with a light rainfall observed on 11th August 2014 with a start at 02:24 am (top) and a heavy rainfall observed on 29th August 2014 with a start at 02:56 pm (bottom). Predicted discharges at a confidence level of 90% are shown as grey bands. The dashed line represents median prediction for a given timestep. Observed discharges are shown as circles (blue if within the prediction bounds, red if outside).

Na hydrogramu vybrané mírné události (obr. 3) vidíme, že pro 3 soubory srážkových dat jsou výsledky velmi podobné, i k nesprávným předpovědím

dochází ve stejné částech hyrogramu (začátek stoupající větve). Výjimkou jsou předpovědi získané pomocí dat z MV spojů se základním zpracováním, kde je evidentní tendence podhodnocovat průtoky, nicméně i zde je dynamika události zachycena velmi dobře.

Příklad silné srážko-odtokové události (obr. 4) nám ukazuje odlišné chování, než tomu bylo u mírných událostí. Nejhorší předpověď, konkrétněji výrazně podhodnocení maximálního průtoku, vznikla po použití dešťových dat ze tří vzdálených srážkoměrů. Ostatní tři soubory srážkových dat, včetně těch z MV spojů se základním zpracováním, vedli k předpovědím velice dobrým ve všech ohledech.

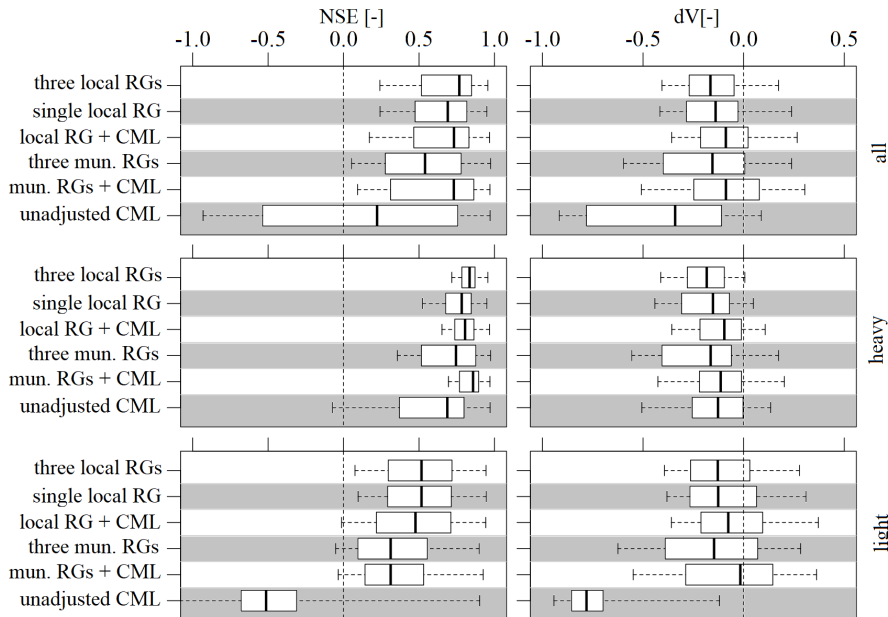


Figure 4.2: Boxplots all 10 events.

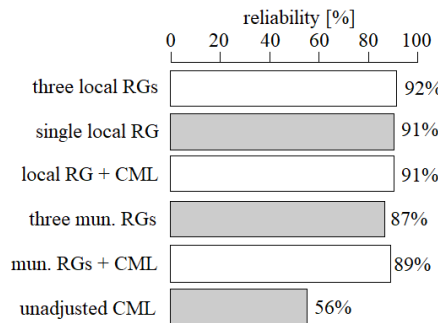
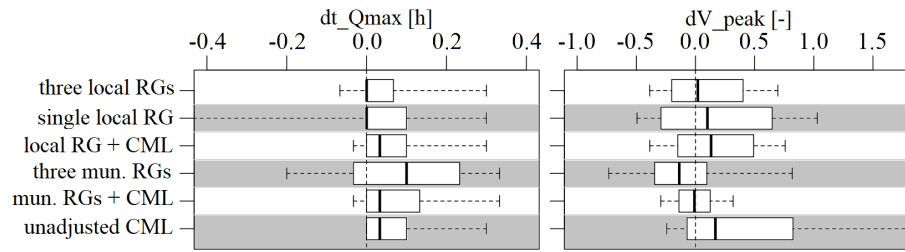


Figure 4.3: Discharge prediction reliability.

**Figure 4.4:** Boxplots heavy rainfalls.

4.4 Discussion

We acknowledge that this approach, not varying the internal relative structure for the given parameter, might be perceived as questionable and could be avoided by introducing additional stochastic parameters, which would incorporate random changes into the internal proportions of the θ parameters. However, we choose not to implement this for the sake of modelling simplicity (lower number of parameters).

Chapter 5

The effect of link characteristics and their position on runoff simulations

This study addresses the ability of individual commercial microwave links (CMLs) to provide relevant quantitative precipitation estimates (QPEs) for urban rainfall-runoff simulations and specifically investigates the influence of CML characteristics and position on the predicted runoff. QPEs from real world CMLs are used as inputs for urban rainfall-runoff predictions and subsequent modelling performance is assessed by comparing simulated runoffs with measured stormwater discharges. The results show that model performance is related to both the sensitivity of CML to rainfall and CML position. The bias propagated into the runoff predictions is inversely proportional to CML path length. The effect of CML position is especially pronounced during heavy rainfalls, when QPEs from shorter CMLs, located within or close to catchment boundaries, better reproduce runoff dynamics than QPEs from longer CMLs extending far beyond the catchment boundaries. Interestingly, QPEs averaged from all available CMLs best reproduce the runoff temporal dynamics. Adjusting CML QPEs to three rain gauges located 2–3 km outside of the catchment substantially reduces the bias in CML QPEs. Unfortunately, this compromises the ability of the CML QPEs to reproduce runoff dynamics during heavy rainfalls.

The bulk of this chapter was originally published in Pastorek et al. (2019b).

5.1 Introduction

Inaccuracies in quantitative precipitation estimates (QPEs) from commercial microwave links (CMLs) are very much dependent on CML's sensitivity to

inaccurate estimation of raindrop-induced attenuation A_r [dB] which is largely determined (see 2.3.1) by its characteristics such as transmission frequency and path length (Leijnse et al., 2008).

Path lengths of CMLs typically range from a few hundred meters up to a few kilometers. Longer CMLs are less prone to bias in CML QPEs caused by inaccurate A_r estimation due to, e.g., imprecise correction for wet antenna attenuation (WAA). However, their path lengths often do not correspond well to relatively small scales of urban (sub)catchments and, thus, they cannot capture rainfall spatial variability at corresponding scales. On the other hand, shorter path lengths, fitting the typical urban catchment scale well, make CMLs more prone to bias. Nonetheless, shorter CMLs typically operate at higher frequencies which are associated with a lower liability to bias.

Unfortunately, very little is known about the combined effect of the CML characteristics and their spatial representativeness on efficient use of CML QPEs for hydrological applications such as rainfall-runoff modeling. This study addresses the above knowledge gap and investigates in how far CML instrumental parameters and network topology influence the performance of CMLs as rainfall sensors for hydrological modelling. This complex problem is addressed in three steps:

1. The sensitivity of QPEs to the CML path length and transmission frequency is analyzed.
2. The CML spatial representativeness related to their path length, position, and the spatial structure of the rainfall event are investigated.
3. As, in theory, CML QPEs should outperform point measurements from rain gauges during extreme or heavy rainfall, we analyze the performance of CML QPEs in such conditions in greater detail.

In our view, main innovations of the study include also the following:

1. It is among the very first which investigate the potential of CML QPEs for urban rainfall-runoff modelling at catchment scales;
2. It employs a unique real-world data set which was collected over three consecutive summer seasons and which contains comprehensive, high-resolution data from a dense network of 19 CMLs; and
3. It provides specific recommendations on how to select CMLs suitable for urban rainfall-runoff modelling.

5.2 Methods

QPEs from real-world CMLs (3.1) are used as inputs in a calibrated urban rainfall-runoff model (3.2). The model performance is evaluated for CML QPEs from various observation layouts by comparing the simulated runoffs with those observed at the stormwater drainage system outlet. Next, we perform an exploratory data analysis on CML attributes to better understand their influence on volumes and temporal dynamics of the simulated runoff.

5.2.1 Data availability

Due to outages in data from the monitoring devices, it was possible to perform and evaluate rainfall-runoff simulations for 71 events from the monitoring period (3.1). For each of the events, there were data available from between 9 and 17 CMLs (47%–89%). To improve the robustness of the statistical evaluation, we have excluded from the analysis 12 rainfall events with less than two thirds of the CMLs available. Also, we excluded three extreme rainfall events for which runoff predictions were unsatisfactory, i.e. maximal discharges were overestimated by more than 100% when modelled using high-quality rainfall data from the three local rain gauges (Fig. 3.1). Similarly, three CMLs (#1, #2, #10), which experienced long outages during the experimental period, are not analyzed in the study. In summary, after rigorous quality control, the analysis is performed for 16 CMLs and 56 events. Details on the rainfall event characteristics are provided in Appendix ??.

5.2.2 From signal levels to QPEs

Although we deliberately chose a pragmatic approach to derive CML QPEs, several steps are necessary to estimate precipitation-induced attenuation for a given CML and to derive the associated precipitation rates:

1. The difference between the transmitted and received signal level $TRSL$ [dB] is calculated for each of two CML channels.
2. A quality check is performed to identify erratic CML behavior which has to be filtered out. The following behavior is regarded as erratic:
 - Sudden peaks where, within two time steps, $TRSL$ increases and then decreases (or vice versa) by more than 5 dB,
 - Longer periods (days) with no signal fluctuation, and
 - Periods with random noise larger than 2 dB.

- 3. TRSL data are aggregated to regular 1-min time series by averaging values within 1-min intervals.
- 4. TRSL time series from the two CML channels are averaged.
- 5. Baseline attenuation B is estimated with a low-pass filter parameter $m = 0.00145$ (Fenicia et al., 2012) and separated from TRSL (Eq. 2.1).

After the baseline separation, we proceed by applying WAA correction (A_{wa} from Eq. 2.2) and calculating the rainfall intensity R [mm/h] (Eq. 2.1) in two different ways:

- WAA A_{wa} is modelled as a constant offset with values suggested by Overeem et al. (2011). Parameters α and β are chosen in accordance with ITU Radiocommunication Sector (2005).
- The mean of the instantaneous R values of the three municipal rain gauges closest to the catchment (Fig. 3.2), aggregated to 15-min time steps, is used for adjusting A_{wa} and α , while keeping $\beta = 1$, as proposed by Fencl et al. (2017).

█ 5.2.3 Observation layouts and their evaluation

Rainfall data from 18 different observation layouts are used as precipitation inputs into the rainfall-runoff model. The rainfall model input is in all cases implemented as areal rainfall in the model meaning that rainfall intensity in a given time step has a constant value over all subcatchments of the model.

Firstly, we employ QPEs derived from only a single CML at a time, using each of the 16 CMLs consecutively. Next, we construct a time series calculated as the arithmetic mean of all available CML QPEs (not weighted) for every time step. These 17 observational layouts based on the CML data are used for both methods of deriving CML QPEs (see the end of section 5.2.2). Additionally, to compare CML QPEs with a traditional way of rainfall monitoring, the mean of the three rain gauges from the municipal network is used as the model input. These are the same rain gauges as those used for CML adjusting, but the original 1-min resolution is used in this case.

The rainfall-runoff simulations are not performed continuously for the whole observation period, but only for individual rainfall-runoff events. The model performance is evaluated, for the 18 studied observation layouts, both CML QPE deriving methods, and each of the 56 events, by comparing the simulated runoffs and observed stormwater discharges. Performance metrics are Nash–Sutcliffe efficiency NSE [-], the Pearson correlation coefficient PCC [-], and the relative error of the total runoff volume dV [-].

The model performance for the rainfall observation layouts is analyzed also with respect to rainfall intensities of evaluated events. For these purposes, we classify the events into “light”, “moderate” and “heavy” (Table 5.1). Runoff simulations for heavy rainfalls are investigated in more detail to demonstrate the ability of CMLs for capturing heavy rainfalls, which are often characterized by high spatial variability and thus difficult to measure reliably with point rain gauge observations. However, we expect that location and spatial scale of CMLs might play a larger role than their instrumental errors when used for modelling runoff generated by heavy (spatially variable) rainfalls.

	Light	Moderate	Heavy
Defining $R_{max,10}$ [mm/h]	$x \leq 5$	$5 < x < 12$	$12 \leq x$
Number of events	20	20	16

Table 5.1: Categorization of rainfall events. The defining maximal 10-min rainfall intensity $R_{max,10}$ as measured by the three rain gauges temporarily installed in the catchment. For detailed info see Supplementary material.

5.2.4 Data uncertainty

To interpret correctly the study results, it is crucial to estimate expected errors of both CML QPEs and discharge measurements. The errors in CML QPEs are addressed in section 2.3.1. The uncertainty of the measured discharges at the outlet of the catchment are estimated following the suggestions of Muste et al. (2012). The discharge is computed from pipe radius R [m], measured flow depth h [m], and measured cross sectional velocity V [m/s], which are assumed to have uncorrelated errors. The following values of input variables are propagated: $R = 0.75$ m with a standard uncertainty (at a 68% level of confidence) $u(R) = 0.0015$ m. The discharge uncertainty is estimated only for periods with stormwater runoff, therefore, we assume that the standard uncertainty of measured flow depth h is $u(h) = 0.015$ m. The standard uncertainty of the flow velocity V in the cross section is estimated as $u(V) = 0.05V$. Finally, the expanded uncertainty (at a 95% level of confidence) of measured discharge $U(Q)$ is estimated for all discharge measurements. The expanded uncertainty $U(Q)$ varies for different flow depths, e.g. for 10% pipe filling, $U(Q) = \pm 0.0282$ m³/s, what is equivalent to $\pm 31.0\%$ of the total value $Q = 0.091$ m³/s. For 50% pipe filling, the uncertainty $U(Q) = \pm 0.245$ m³/s, corresponding to ($\pm 11.0\%$) of the discharge $Q = 2.17$ m³/s.

5.3 Results

Firstly, typical features of simulated discharge are illustrated on a hydrograph of one of the 56 events. Secondly, the performance of the rainfall-runoff model

is investigated in relation to the CML lengths and frequencies. Afterwards, the model performance is evaluated separately for heavy rainfalls to understand the effect of CML lengths and positions during spatially more variable rainfalls. Finally, runoff simulations for CML QPEs adjusted to rain gauges are presented.

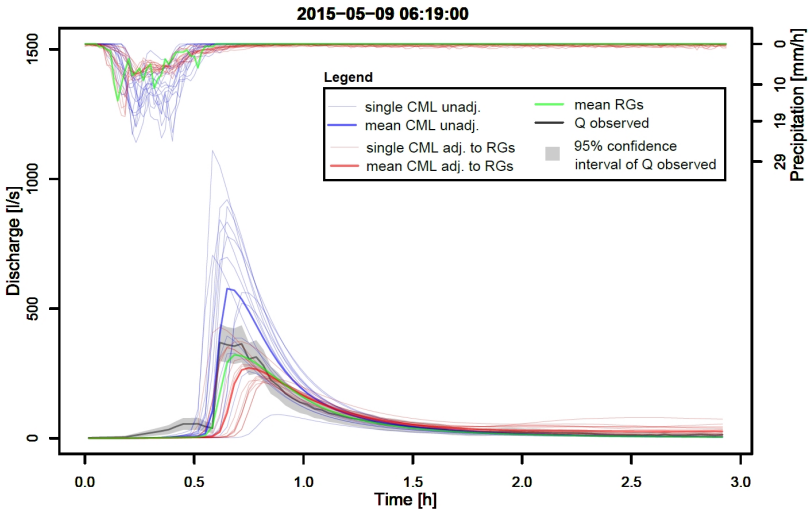


Figure 5.1: Modelled and observed discharges for a selected rainfall-runoff event and all examined rainfall observation layouts: QPEs from individual CMLs both unadjusted (“single CML unadj.”) and adjusted to rain gauges (“single CML adj. to RGs”); The mean of both unadjusted and adjusted QPEs from all available CMLs (“mean CML unadj.” and “mean CML adj. to RGs”); The mean of the three municipal rain gauges (“mean RGs”).

5.3.1 Characteristic features of simulated hydrographs

A hydrograph which illustrates well typical features of the rainfall-runoff process is shown in Fig. 5.1 (see Supplementary material for hydrographs of all rainfall-runoff events). Firstly, one can see that discharge simulations using unadjusted CML QPEs (in blue) can be highly biased, however, this bias varies substantially for various individual CMLs (dV between -0.709 and 0.823). In contrast, the correlation with the observed runoff is relatively high (PCC 0.878 in mean) and much more stable among various CMLs (0.15 in st. dev.). Secondly, the efficiency of adjusting CML QPEs to rain gauge observations (in red) is highly conditional on the rain gauge data. The adjustment reduces the bias in simulated discharges (dV between -0.280 and 0.066), but it does not always outperform simulations based on the mean of the rain gauges (dV -0.152). Moreover, if the rain gauges do not capture rainfall temporal dynamics well, adjusted CML QPEs also perform poorly,

and the correlation of predicted and observed runoff is lower than without the adjustment (see Appendix ???, events from 2014-10-16 or 2015-09-09).

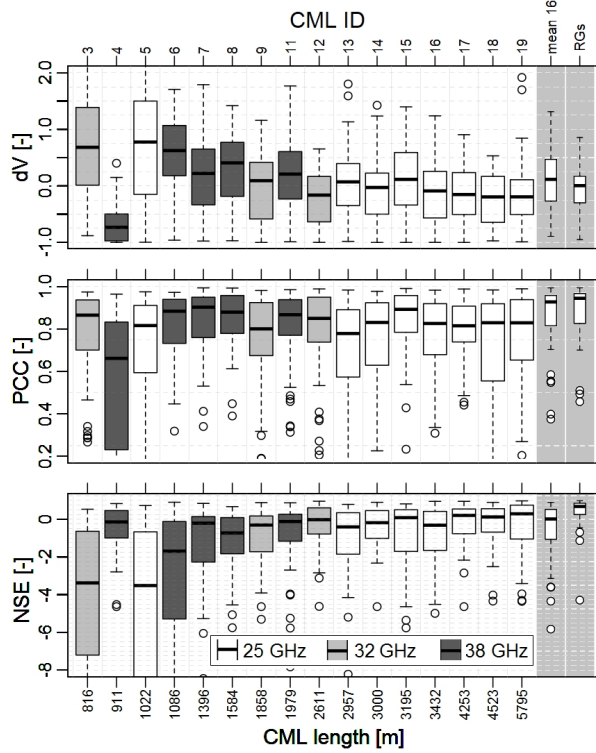


Figure 5.2: Boxplots of performance metrics (see 5.2.3) obtained using unadjusted CML QPEs, summarized for all available rainfall-runoff events. "Mean 16" stands for the mean of all QPEs from all 16 individual CMLs, "RGs" stands for the mean of the three municipal rain gauges. Boxes represent the interquartile range, whiskers extend to the most extreme data point which is no more than 1.5 times the interquartile range from the box, and circles represent outliers.

5.3.2 Performance in relation to CML lengths and frequencies

Fig. 5.2 shows boxplots of the model performance when using unadjusted CML QPEs for all 56 rainfall-runoff events, where each boxplot belongs to one observation layout. The layouts are sorted by the CML path length. Predicted discharges are on average highly biased and the large whiskers indicate substantial inter-event variability outside the upper and lower quartiles for all metrics. The largest dV values tend to be associated with unadjusted QPEs from short CMLs (the exception of CML #4 is discussed below). Similarly, the inter-event variability in dV is largest for simulations with short unadjusted CMLs. Such positive bias linked to the high sensitivity of short CMLs to wet antenna attenuation has been observed in the past (e.g. Fencl et al., 2019).

CML #4 is a distinctive exception to the observations formulated above. Although it is very short, unadjusted QPEs from this CML lead to substantially underestimated runoff volumes. Additional analyses identified malfunction in one of the two channels of this CML causing unusually low values of observed attenuation. Since we use the mean of the observed attenuation of the two channels to estimate rainfall intensity, the intensities derived from this CML, and consequently the simulated runoffs, are systematically underestimated.

The model performance in terms of *PCC* (Fig. 5.2, middle), which is insensitive to linear bias, does not show a clear dependence on CML path lengths. Better-than-average values are obtained using QPEs from 38 GHz CMLs. This is probably because these CMLs cover the catchment relatively well while being more sensitive to rainfall than lower frequency CMLs. Interestingly, the best performing CML QPEs, with *PCC* values similar to the rain gauges, are those derived from the mean of all available CMLs. *NSE* values (Fig. 5.2, bottom) are generally unsatisfactory, due to the high bias in the unadjusted CML QPEs. As expected, *NSE* values are better for longer CMLs and for the mean of QPEs from all 16 CMLs.

Using the given CML network topology, the relation between the CML frequency and its performance cannot be studied completely independently of the CML path length. Nevertheless, results of CMLs #9 and #11 or #12 and #13, which have similar lengths but different frequencies, indicate that higher frequencies (which are more sensitive to raindrop attenuation) tend to provide better results, especially in terms of better correlations.

In general, when evaluating discharge simulations using volume-related performance metrics (*dV* and *NSE*), instrumental errors seem to dominate over errors related to CML spatial representativeness. The longest least biased CMLs distinctively outperform shorter CMLs. The short CMLs are within or close to the catchment boundaries, and their lengths correspond better to the catchment scale (Fig. 3.2), but they are more prone to bias due to wet antenna attenuation (see 2.3.1). On the other hand, correlations are slightly better for shorter 38 GHz CMLs than for longer 26 GHz CMLs. However, the spatial representativeness of CMLs in relation to the catchment area might be more pronounced during heavy rainfalls, which are typically highly spatially variable and during which we can expect CMLs to be relatively less prone to instrumental errors (see 2.3.1). This is investigated in greater detail in the following subsection.

5.3.3 Performance during heavy rainfalls

Fig. 5.3 summarizes the rainfall-runoff modelling performance for heavy rainfalls. General tendencies for volume-related statistics are similar as when summarizing for all available events. It can be seen that there is still a

considerable dependency between the CML path length and the bias in simulated discharges (dV , Fig. 5.3, top), which also affects the performance in terms of NSE (Fig. 5.3, bottom). Interestingly, the temporal dynamics (PCC , Fig. 5.3, middle) are now best reproduced (median PCC 0.94, st. dev. 0.04) by the mean of all CML QPEs. This suggests that such averaged data contain valuable information about the rainfall spatiotemporal dynamics above the catchment. For the individual CML QPEs, the highest PCC values are reached by QPEs from relatively short 38 GHz CMLs (#6, #7, #8) located in the western part of the catchment. This demonstrates that even biased CML QPEs can very well reproduce runoff dynamics if the CMLs cover the catchment area well. Nevertheless, the bias in the QPEs from short CMLs considerably limits their performance in terms of volume-related performance metrics, which are important for applications such as modelling of water balance or designing large retention tanks. Elimination of the bias in CML QPEs by adjusting to rain gauges is presented in the next section.

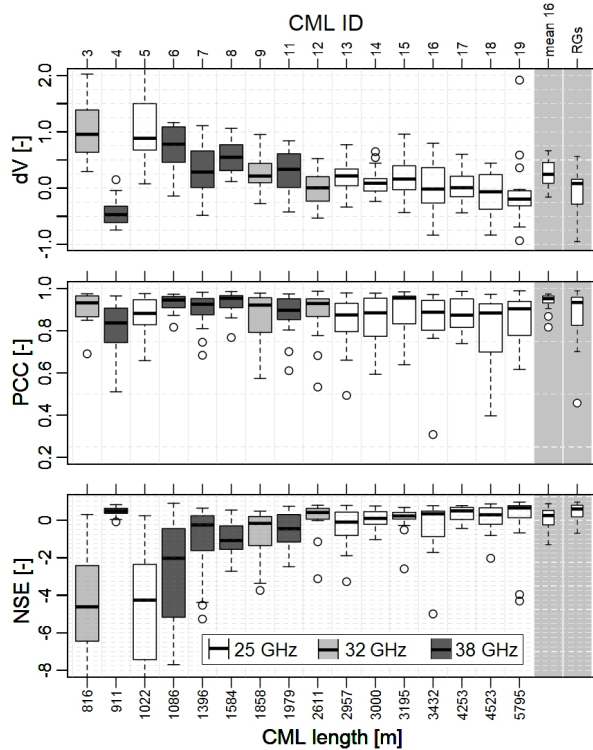


Figure 5.3: Boxplots of performance metrics obtained using unadjusted CML QPEs, summarized only for heavy rainfalls. "Mean 16" stands for the mean of all QPEs from all 16 individual CMLs, "RGs" stands for the mean of the three municipal rain gauges. Boxes represent the interquartile range, whiskers extend to the most extreme data point which is no more than 1.5 times the interquartile range from the box, and circles represent outliers.

5.3.4 Discharge simulations from adjusted CML QPEs

Although the adjustment of CML QPEs to rain gauges greatly reduces the bias (median dV between 0.01 and 0.12; boxplots presented in Fig. S3 in the Supplementary material), it does not outperform the rain gauge data (median dV 0.01). There are no clear trends associated with CML path length, neither in terms of the dV median nor the dV inter-event variability (st. dev. between 0.37 and 0.61). Similarly, for all CML QPEs, correlations of simulated and observed discharges are in similar ranges as for the rain gauges used alone (PCC medians around 0.9, st. dev. around 0.27). For six of the individual CMLs (including short ones) and for the mean of all CMLs, the adjusted QPEs lead to slightly less variable NSE values than the rain gauges (st. dev. between 0.6 and 0.73). However, no CML QPEs lead to decisively higher median NSE values.

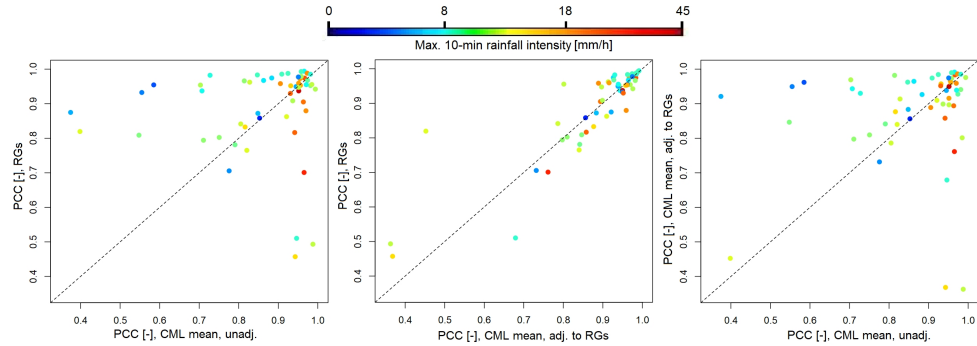


Figure 5.4: Scatterplots of PCC with color-coded max. 10-min rainfall intensities ($R_{max,10}$) of individual events. Left: The mean of unadjusted CML QPEs (x axis) vs. rain gauges (y axis). Middle: The mean of adjusted CML QPEs (x axis) vs. rain gauges (y axis). Right: The mean of unadjusted (x axis) and the mean of adjusted CML QPEs (y axis).

Adjusting CML QPEs to rain gauge data effectively minimizes the bias in the CML QPEs, though it is considerably constrained by the reliability of the rain gauge data. This is especially critical during heavy rainfalls when observations from rain gauges located 2–3 km from the catchment often do not represent rainfall intensities directly in the catchment. In these cases, adjusted CML QPEs tend to be unreliable and can even worsen CML performance, especially in terms of their ability to capture temporal dynamics of rainfall and subsequent runoff. This is demonstrated in Fig. 5.4, where discharge simulations based on *i*) only rain gauges, *ii*) the mean of all unadjusted CML QPEs, and *iii*) the mean of all adjusted CML QPEs are evaluated in terms of PCC and compared with each other. For heavy rainfall events, the unadjusted CML QPEs clearly outperform the rain gauge data (Fig. 5.4, left). Adjusting CML QPEs to rain gauges improves the PCC performance for light and moderate rainfall events, but it also worsens the results for heavy

(and a few moderate) rainfall events (Fig. 5.4, right). When comparing the adjusted CML QPEs and the rain gauge data (Fig. 5.4, middle), there is no clear difference between the respective *PCC* values.

5.4 Discussion

Our experimental results on using QPEs from CMLs for urban rainfall-runoff predictions suggest that CMLs can indeed provide valuable rainfall data. However, if CML QPEs are not adjusted to rain gauges, the large bias in CML QPEs leads to unsatisfactory performance, especially for short CMLs. Nevertheless, the results strongly depend on the reliability of the rainfall-runoff model and discharge observations, the pre-processing method applied to obtain CML QPEs, and the quality and availability of the CML data. Therefore, to better interpret our results, it is necessary to discuss *i*) the combined effect of uncertainty in measured discharges and the rainfall-runoff model on overall performance of CML-based discharge simulations, *ii*) CML preprocessing with a special focus on eliminating the bias in CML QPEs, and *iii*) the effect of the quality and availability of CML QPEs on the representativeness of the results and their transferability to different catchments.

The rainfall-runoff model was validated using independent rainfall observations from three rain gauges located within or close to the catchment boundaries (Fig. 3.1, left) for all events analyzed in this study. This enables us to directly quantify the reliability of the model (see section 3.2). The validation shows that the model reproduces runoff very well in terms of both discharge volumes (dV) and temporal dynamics (*PCC*, partly *NSE*). The relative error in dV is small for most of the evaluated events (mean -0.007, st. dev. 0.153). These values are more than a magnitude lower than those obtained using unadjusted QPEs from short CML, and about two times lower in comparison to those of the best performing CML. Therefore, the bias in CML-based discharge simulations can be attributed mostly to the uncertainty (the bias) in CML QPEs and not to the combined uncertainty of observed discharges and the rainfall-runoff model. The validation also shows that the simulated discharges are highly correlated with the observed ones (mean 0.95, st. dev. 0.06). The mean *PCC* for CML-based discharge simulations is between 0.49 and 0.86, with st. dev. between 0.15 and 0.43. Thus, the deficit in reproducing runoff dynamics can also be attributed predominantly to uncertainties in CML QPEs. The only exception are discharge simulations for heavy rainfalls obtained from the mean of all unadjusted CML QPEs (Fig. 5.3, boxplot ‘mean 16’), for which *PCC* values are comparable (mean 0.94, st. dev. 0.04) to the excellent runoff predictions using the local rain gauges (mean 0.96, st. dev. 0.02). In summary, the validation of the rainfall-runoff model demonstrates that the combined uncertainty related to measured discharges

and the rainfall-runoff model introduces only very little variability and, most importantly, no systematic errors into the performance assessment.

Results of this study show that bias in unadjusted CML QPEs negatively affects their usefulness for rainfall-runoff modelling, especially in terms of volume-related statistics. Most importantly, unadjusted QPEs were increasingly overestimated as CML path length decreased since shorter CMLs are relatively more sensitive to errors in A_r estimation (2.3.1) due to, e.g. inaccurate WAA correction (Eq. 2.2). In our pragmatic rainfall retrieval approach, WAA A_{wa} was considered constant and its value was taken from literature (Overeem et al., 2011). It can be expected that calibrating the WAA model using independent rainfall data, or stormwater runoff measurements which reflect transformed rainfall aggregated for a whole catchment well (Pastorek et al., 2019a), would result in less biased QPEs, on average. However, the large inter-event variability indicates that the simple wet antenna correction with a constant threshold is not satisfactory, and more precise WAA models (e.g. with WAA A_{wa} proportional to rainfall intensity) are necessary to obtain unbiased CML QPEs.

Adjusting CML QPEs to measurements from traditional rain gauges (Fencl et al., 2017) successfully minimizes the bias. However, using adjusted CML QPEs does not outperform predictions based on rain gauge data. Moreover, the adjustment considerably worsens the ability of CML QPEs to reproduce runoff dynamics during heavy rainfalls, except for QPEs from long individual CMLs with end nodes located further from the catchment than rain gauges. This is because the adjustment method strongly depends on the reliability of rain gauge observations which are often too far from each other to accurately observe small-scale rainfall variability. Thus, although the adjusting is conceptually promising for eliminating the bias, it requires further development. One important advantage of the adjustment suggested by Fencl et al. (2017) is that, thanks to the high temporal resolution of CML QPEs, it performs well also for rain gauge data with hourly resolution. Thus, this method can be recommended for disaggregating rainfall data in catchments where rain gauge data are available only in temporal resolutions suboptimal for urban drainage modelling.

We show that runoffs simulated using QPEs from (relatively short) CMLs located within or close to the catchment boundaries are, in spite of being biased, very well correlated with the observed runoffs. Moreover, in this respect they outperform runoffs simulated using the relatively unbiased QPEs from long CMLs, primarily during heavy rainfalls. This is probably because heavy rainfalls are often characterized by high spatial variability, and the paths of the long CMLs extend far beyond the catchment. Thus, these long CMLs cannot accurately capture areal rainfall over the catchment. For larger catchments, even relatively long CMLs might not extend out of the catchment, and thus they could be better suited to provide representative

rainfall information. However, larger catchments might also require spatially distributed rainfall information, and assuming uniform rainfall, as in our study, might provide unsatisfying results. On the other hand, our results show that averaging unadjusted QPEs from all available CMLs best reproduces runoff dynamics, probably because it best captures the temporal variability of areal rainfall over the catchment, even though the averaging concerns a substantially larger area. This is in accordance with the findings of Ochoa-Rodriguez et al. (2015), who identified temporal variability of rainfall as the most sensitive attribute for urban rainfall-runoff simulations. Therefore, it can be expected that CML QPEs will be suitable for modelling runoff dynamics also in other urban catchments where CML coverage corresponds to the spatial extent of typical rainfalls.

5.5 Conclusions

This study has evaluated the suitability of quantitative precipitation estimates (QPEs) from commercial microwave links (CMLs) for urban rainfall-runoff modelling. Using a unique data set from three summer seasons collected in a small (1.3 km^2) urban catchment in Prague-Letňany, runoff observed in the catchment was compared to runoff predicted using rainfall data from different observational layouts, in particular QPEs derived from various individual CMLs. We used a hydrodynamic model which accurately describes the rainfall-runoff process, although it underestimates flows for extreme events. The results have demonstrated that CML QPEs can be conveniently used for rainfall-runoff modeling. However, the CML data pre-processing, characteristics of the individual CMLs, such as frequency or path length, and their position influence the quality of the retrieved QPEs. The main conclusions are as follows:

- The sensitivity of CMLs to rainfall, which is given by their frequency, polarization, and length, is the most influential factor affecting the accuracy of CML QPEs, especially their bias, i.e. systematic under- or overestimation. This bias is greatest for the shortest CMLs, however, it is also variable among events. Thus, the ability of such biased CML QPEs to provide reliable flow estimates is predominantly low.
- As expected, the position of CMLs within the small urban catchment affects their ability to capture rainfall-runoff dynamics, such as the onset of a runoff event, timing of the hydrograph rising limb, runoff peak, and recession limb. The effect of CML position is especially pronounced for heavy rainfalls, when shorter CMLs with paths within or close to the catchment boundaries reproduce runoff dynamics better than longer CMLs extending far beyond the catchment.

- The best performance in terms of capturing runoff dynamics is obtained when rainfall observations of all CMLs are averaged. Notably promising results are obtained during heavy rainfall events, probably because areal rainfall from all the CMLs captures the temporal rainfall variability especially well, and runoff dynamics in small urban catchments are often more sensitive to temporal than spatial variations. Therefore, averaging of CML QPEs can be especially recommended for applications where the temporal structure of runoff and timing of peak flows is more important than volume-related statistics, e.g. alarms during sewer construction/maintenance works.
- Adjusting the CML QPEs to data from rain gauges substantially reduces their bias while minimizing the difference among CMLs of various characteristics. Unfortunately, the adjustment also considerably worsens the ability of CML QPEs to reproduce runoff dynamics during heavy rainfalls, except for QPEs from long individual CMLs. On the other hand, the adjustment can be recommended for disaggregating rainfall data in catchments where traditional rainfall data are available only in temporal resolutions suboptimal for urban drainage modelling.
- Our experimental results demonstrate that CMLs cannot replace observation networks designed for long-term continuous hydrological monitoring. Many events had to be excluded from the analysis because of the limited CML data availability due to removal or replacement of CML units, communication outages, or hardware malfunctions, to name just a few challenges. Nevertheless, CMLs can very well complement the traditional networks and provide valuable data for operational hydrology. We expect that this is especially the case for sparsely gauged or completely ungauged regions.

Reducing systematic errors in CML QPEs remains a major challenge compromising their applications in water management tasks where runoff volume is essential, e.g. water balance modelling or designing retention capacity of drainage systems. CML QPE preprocessing methods tailored to different water management tasks, catchments, and CML networks could solve this problem. Therefore, it is necessary to better understand the interactions between the CML QPE observation errors and catchment runoff characteristics. Although modelling studies with virtual drop size distribution fields (Fencl et al., 2013) can be useful to investigate topological issues, more monitoring campaigns and experimental case studies are necessary to understand error-generating processes related to CML hardware, such as antenna wetting.

Chapter 6

Practical Approaches to Wet-Antenna Correction

This study analyzes how, when deriving quantitative precipitation estimates (QPEs) from commercial microwave links (CMLs), wet antenna attenuation (WAA) can be corrected without dedicated rainfall monitoring. For a set of 16 CMLs, the performance of six empirical WAA models was studied, both when calibrated to rainfall observations from a permanent municipal rain gauge network and when using model parameters from the literature. The transferability of WAA model parameters among CMLs of various characteristics was also addressed. The results show that high-quality quantitative precipitation estimates with a bias below 5% and RMSE of 1 mm/h in the median could be retrieved, even from sub-kilometer CMLs where WAA is relatively large compared to raindrop attenuation. Models in which WAA is proportional to rainfall intensity provide better WAA estimates than constant and time-dependent models. It is also shown that the parameters of models deriving WAA explicitly from rainfall intensity are independent of CML frequency and path length and, thus, transferable to other locations with CMLs of similar antenna properties.

The bulk of this chapter was originally published in:

Pastorek, J., Fencl, M., Rieckermann, J., Bareš, V. 2021. **Precipitation Estimates from Commercial Microwave Links: Practical Approaches to Wet-Antenna Correction.** *IEEE Transactions on Geoscience and Remote Sensing* XYZ, XYZXYZ.
<https://doi.org/10.1109/TGRS.2021.3110004>.

6.1 Introduction

The complexity of the antenna (radome) wetting process, namely its dependence on antenna hardware properties (e.g. coating; van Leth et al., 2018) and on atmospheric conditions other than precipitation, is a major challenge to reliable estimation of wet antenna attenuation (WAA). It also negatively affects the transferability of WAA models among different commercial microwave links (CMLs) and, thus, optimal WAA models should ideally be determined for each individual CML. This is especially true for models whose parameters depend on CML path length (e.g. Kharadly & Ross, 2001). However, optimal WAA model identification (e.g. for calibration purposes) on the level of individual CMLs is challenging for real-world application with networks consisting of a high number of CMLs. As noted by (Ostrometzky et al., 2018), maintenance of dedicated equipment for the retrieval of the needed reference rainfall observations is impractical for such networks. Consequently, application-focused studies with city or regional-scale CML networks have often not applied any WAA correction at all (Chwala et al., 2012; Smiatek et al., 2017) or have used only a simple constant offset model (Pastorek et al., 2019b; Overeem et al., 2011; Roversi et al., 2020; Fencl et al., 2020). Although the latter approach may be a reasonable choice when observations of the difference between the transmitted and received signal levels $TRSL$ [dB] are available only as 15-min maxima and minima (Chwala & Kunstmann, 2019), it can introduce considerable bias in resulting CML quantitative precipitation estimates (QPEs) (Pastorek et al., 2019b; Fencl et al., 2019). To avoid such errors, Graf et al. (2020) recently tested a time-dependent (Schleiss et al., 2013) and a semi-empirical WAA model assuming a homogeneous water film on antenna radomes which depends on rain rate through a power law (Leijnse et al., 2008). However, in the case of both WAA models, only a single set of fixed parameters for all of around 4000 CMLs from their extensive dataset was used and this did not address the suitability of the WAA model parameters for individual CMLs.

This study analyzes, for the first time, six empirical WAA models, including a newly proposed one, based on considerably different assumptions and tests their performance in detail. In contrast to previous studies, often limited by a low number of CMLs investigated (Schleiss et al., 2013; Leijnse et al., 2008; van Leth et al., 2018), short time series of a few months (Leijnse et al., 2008; Overeem et al., 2011; Roversi et al., 2020) or 15-min CML data sampling intervals (Overeem et al., 2011; Rios Gaona et al., 2018), a rich dataset of more than two years of data retrieved from 16 CMLs with a sub-minute sampling rate is used. Motivated by the vision of reducing the costs of future studies with high numbers of CMLs, we also address the previously recognized need (Ostrometzky et al., 2018; Graf et al., 2020) to minimize the amount of auxiliary data necessary for WAA estimation without compromising the quality of retrieved QPEs and, thus, we introduce three

conceptual innovations not previously presented in relevant literature. Firstly, we show how the investigated empirical WAA models can be calibrated while notably minimizing the requirements on the reference rainfall data necessary, i.e. using only a rain gauge network with a spatial resolution of one gauge per $20-25 \text{ km}^2$ and a temporal resolution of 15 minutes. Secondly, we analyze the variability in WAA model parameters optimized for different CMLs, thus indirectly assessing parameter uncertainties, and investigate which of the studied models can provide reliable WAA estimates without being calibrated for each individual CML. This includes a reformulation of a previously reported WAA model (Valtr et al., 2019). Thirdly, we suggest a procedure enabling the application of rainfall-dependent WAA models without any auxiliary rainfall observations, i.e. using only CML data.

6.2 Methods

Attenuation data from 16 CMLs collected over a 3-year period (3.1) are processed (6.2.1) and corrected for WAA using six empirical WAA models (6.2.2). The resulting CML QPEs are evaluated against the rain gauge data from the municipal network (6.2.3).

6.2.1 From signal levels to QPEs

CML data processing steps before baseline separation, including a quality check and aggregation to a 1-min resolution, are done in the same way as described in section 5.2.2. Baseline attenuation B [dB] is assumed to equal $TRSL$ [dB] (Eq. 2.2) during dry periods. During wet periods, B is estimated by linearly interpolating from the dry periods. Data available from both CMLs and rain gauges for the wet period identification are used. First, we identify wet timesteps for the CML data (mean $TRSL$ of all CMLs) using a climatological threshold [20] defined as the 90th percentile of the rolling standard deviation of a 60-minute window. For the rain gauge data, timesteps are identified as wet when gauge tipping is observed at one or more gauges. Subsequently, wet periods are defined for both sensor types by setting the start of a wet period to one minute before the first observed wet timestep and the end to 60 minutes after the last one to ensure that baseline interpolation is not affected by wet antennas. Afterwards, the wet periods defined by the two sensor types are merged by taking the earliest starts and the latest ends. These are then used for the baseline separation using the linear baseline model.

From the above defined wet periods, only hydrologically relevant rainfall events (total rainfall depth $H > 2 \text{ mm}$) are selected for further processing.

After eliminating events with substantial data gaps, 53 events (360 hours) are available.

After the baseline separation, WAA A_{wa} [dB] is estimated (details in the next section) and subtracted to obtain raindrop attenuation A_r [dB] (Eq. 2.2). Then, A_r is divided by the CML path length and thus transformed into specific raindrop attenuation γ [dB/km] from which rainfall intensity R [mm/h] is calculated using Eq. 2.1, with parameters α and β according to ITU Radiocommunication Sector (2005). These parameter values are in very good agreement with values derived directly from drop size distribution observations (Chwala & Kunstmann, 2019; Valtr et al., 2019), however, they may not be optimal for other rain type regions (Rios Gaona et al., 2018).

6.2.2 Empirical WAA models

We evaluate a scenario without correcting for WAA (Zero) and six empirical models for WAA correction (overview in Table 6.1). For all models, it is assumed that WAA is estimated for two antennas, i.e. at both CML ends. The simplest approach is to model WAA A_{wa} as a constant offset (O; Overeem et al., 2011). In a more complex method, we model A_{wa} as time-dependent, exponentially increasing towards an upper limit during wet periods, and decreasing exponentially afterwards (S; Schleiss et al., 2013).

Next, we evaluate models where A_{wa} depends on R . Valtr et al. (2019) proposed a model (V) where the dependence on R is explicit through a power law

$$A_{wa} = 2k'R^{\alpha'} \quad (6.1)$$

where k' and α' are the power law parameters. We also analyze a model (KR) suggested by Kharadly & Ross (2001) deriving A_{wa} from observed attenuation A [dB], i.e. depending on R implicitly. However, as A is dependent on CML path length, optimal parameters of the KR model would differ for two CMLs with the same hardware but with different path lengths. To eliminate this feature, we propose a model (KR-alt) in which A_{wa} is bounded by an upper limit, as in Kharadly & Ross (2001), but derived from R explicitly through a power law

$$A_{wa} = C(1 - \exp(-dR^z)) \quad (6.2)$$

where C [dB] represents the maximal A_{wa} possible, and d and z are power law parameters. Nevertheless, as optimal C and d values are not independent and can compensate for each other (similar to the KR model, see Fig. 6.4), we reduce the number of parameters to two by setting $d = 0.1$.

WAA models with parameters independent of CML path length can also be formulated when A_{wa} is derived explicitly from γ , not only R . However, it is unclear which of the two alternatives would provide WAA model parameters

independent of CML frequency. Unlike γ , R is independent of CML frequency. The results from Leijnse et al. (2008) suggest that A_{wa} is also considerably less sensitive to CML frequency than A_r or γ . Therefore, parameters of the models deriving A_{wa} from R explicitly are probably more transferrable among frequencies. To confirm this hypothesis, we reformulate the model of Valtr et al. (2019) (V-alt), and replace R with γ so that:

$$A_{wa} = 2p\gamma^q \quad (6.3)$$

where p and q are the power law parameters.

As neither R nor γ can be observed directly using CMLs, the V, V-alt, and KR-alt model equations must be rearranged to include only one unknown variable, A_{wa} , which can thus be quantified from A (details in Appendix). The rearranged equations are then solved numerically.

WAA model	Parameter values from the literature	Abbrev.
Zero WAA (no WAA correction)	—	Zero
Constant non-zero offset	$A_{wa} = 1.585$ dB the mean of the optimal values identified in Overeem et al. (2011)	O
Dynamic (time-dependent) (Schleiss et al., 2013)	$W = 2.3$ dB $\tau = 15$ min from Schleiss et al. (2013)	S
Depending on A explicitly with an upper limit (Kharadly & Ross, 2001)	$C = 8$ dB $d = 0.125$ from Kharadly & Ross (2001); for 27 GHz	KR
Depending on R explicitly with an upper limit	—	KR-alt
Power-law relation to R (Valtr et al., 2019)	$k' = 0.68$ $\alpha' = 0.34$ from Valtr et al. (2019)	V
Power-law relation to γ (reformulated V)	—	V-alt

Table 6.1: Overview of the investigated WAA models and their parameters.

6.2.3 Calibration and performance of WAA models

The WAA models studied are evaluated when using parameter values taken from the literature, if available, and when calibrated to rainfall data from the three municipal rain gauges. Moreover, for each WAA model, calibration is done in three scenarios:

- separately for each of the 16 CMLs;
- separately for each frequency band; and
- for all CMLs at once.

In total, data from 53 rainfall events (360 hours) are available for WAA model calibration and evaluation. From these, we randomly select 25 events (281 hours) for the calibration. Model parameters are optimized by comparing the CML QPEs with the mean R of the three municipal rain gauges. Both data sets are aggregated from a 1-min to a 15-min resolution to reduce observation noise. The root mean square error ($RMSE$) is used as the objective function and optimized with simulated annealing, an optimization method designed for complicated non-linear functions with many local minima (Xiang et al., 2013). For calibration scenarios using multiple CMLs at once, the mean RMSE of the CMLs is optimized.

Once the optimal WAA model parameters are identified, they are used to derive CML QPEs for the remaining 28 events (349 hours) not used for calibration. The CML QPEs are aggregated from the 1-min to the 15-min resolution and evaluated by direct comparison with the rain gauge data (the mean of the three gauges in the 15-min resolution). The QPEs are evaluated individually for each CML using a time series consisting of all 28 events, the performance for individual events is not quantified. Performance metrics employed are:

- the relative error of the rainfall depth dH [%] reflecting the bias;
- the root mean square error $RMSE$ [mm/h]; and
- the Spearman rank correlation coefficient SCC [-] which quantifies the strength of a monotonic relationship between two variables and is independent of both linear and non-linear bias.

6.3 Results

Firstly, the performance of the estimated CML QPEs summarized for all CMLs is presented (6.3.1). Secondly, the QPEs are investigated in closer detail on the level of individual CMLs (6.3.2). Parameter values used for the WAA model evaluation are also presented (6.3.3).

6.3.1 Summary for all CMLs

The results summarized in Fig. 6.1 show that, when calibrated individually for each CML, models in which A_{wa} is proportional to R (KR, V, KR-alt, V-alt) can lead to CML QPEs with a bias lower than 5% in the median (up to 10% for most CMLs) and with $RMSE$ between 0.8 and 1.2 mm/h. Models explicitly relating A_{wa} to R (V and KR-alt) attain similarly good values (median bias less than 5%, standard deviation 18%) not only when

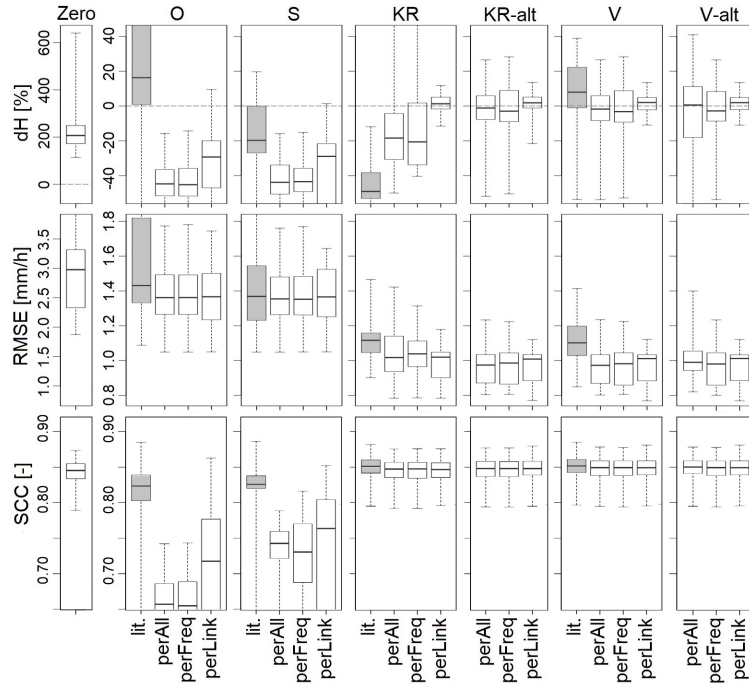


Figure 6.1: Boxplots showing variation in the performance of the QPEs from the 16 individual CMLs quantified by the performance metrics dH (top), $RMSE$ (middle), and SCC (bottom). CML QPEs have been derived without WAA correction (Zero) and using the six WAA models. Sub-boxplots show the effect of WAA model calibration (lit. – parameter values from literature, perAll – calibrated for all CMLs at once, perFreq – calibrated separately for CMLs operating at the three various frequency bands, perLink – calibrated separately for each CML). Note the different ranges of the y-axes for the Zero model.

calibrated individually for each CML, but also when calibrated for groups of CMLs with the same frequency and for all CMLs at the same time. Similarly, $RMSE$ obtained using these two models is almost the same, between 0.8 and 1.2 mm/h, for all three calibration approaches. A very similar performance is reached using the V-alt model, which relates A_{wa} to γ , when calibrating separately for each of the three frequency bands. However, when calibrating the V-alt model for all CMLs at once, the standard deviation of dH increases to 25% and $RMSE$ values reach up to 1.4 mm/h for some CMLs. Calibrating models O and S leads to markedly underestimated dH values for most CMLs (around 40% in median) for all three calibration approaches. This also affects the respective $RMSE$ values which are around 1.4 mm/h in the median for all calibration approaches. Interestingly, using the S model with parameter values from the literature leads to a lower bias for most CMLs (dH -20% in the median). However, the $RMSE$ is virtually the same as for the calibrated model, with only a slightly larger variance. For other WAA models, the literature values perform, in general, worse than those optimized during the calibration, both in terms of dH and $RMSE$. As expected, without the WAA

correction, CML QPEs are considerably overestimated (median dH ca. 200%, $RMSE$ ca. 3 mm/h).

The correlation in terms of SCC (Fig. 6.1 bottom) reaches very similar values (about 0.85 in median) for all WAA models in which A_{wa} is proportional to R (KR, V, KR-alt, V-alt), regardless of whether/how they are calibrated. Only negligibly lower values are reached when not using any WAA model at all (scenario Zero). For most CMLs, SCC values between 0.8 and 0.85 are associated with the O and S models with parameter values from the literature. Calibrating these two models has led not only to a considerable underestimation of rainfall, but also to relatively low SCC values (medians between 0.65 and 0.76).

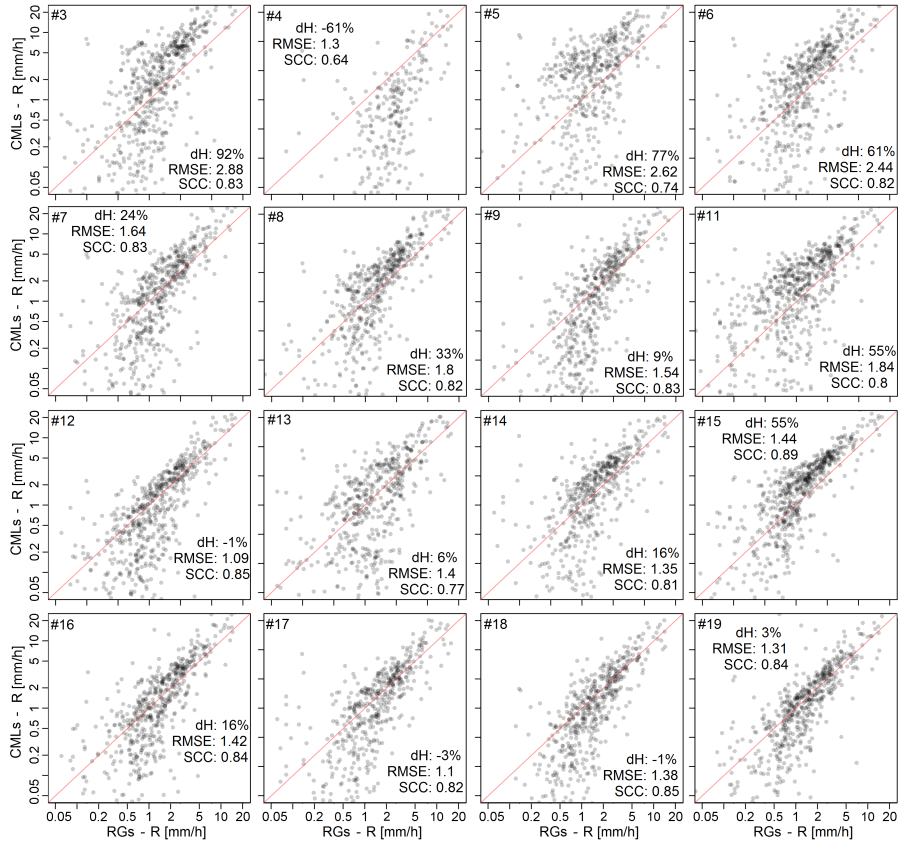


Figure 6.2: Scatter plots comparing rain gauge data (RGs) with CML QPEs for the O model with parameters from the literature. Note that the axes are in logarithmic scales. The presented 15-minute data from the 28 rainfall events used for the evaluation represent 349 hours of observations. In 835 out of the 1,401 time steps, rain gauge data contain non-zero records. Most points with RG rainfall intensity below 0.3 mm/h are out of the plotting range, as the respective CML QPEs are below 0.05 mm/h.

6.3.2 Individual CMLs

In addition, we analyze the estimated QPEs on the level of individual CMLs for two WAA modelling scenarios. First, CML QPEs derived using the commonly used O model with parameter values from literature are compared with the rain gauge data (Fig. 6.2). Next, representing the better performing WAA models from above, the same is done for the V model with parameters optimized for all CMLs at once (Fig. 6.3). The V model leads to a distinct improvement over the O model. The V model reduces the bias for low and high R and thus removes the dependence of errors in CML QPEs on R . Therefore, the performance metrics dH and $RMSE$ are improved for most CMLs, however, the change of SCC is practically negligible. The reduction of errors is most significant for the shortest CMLs, as the relative contribution of A_{wa} to A decreases with the increasing path length.

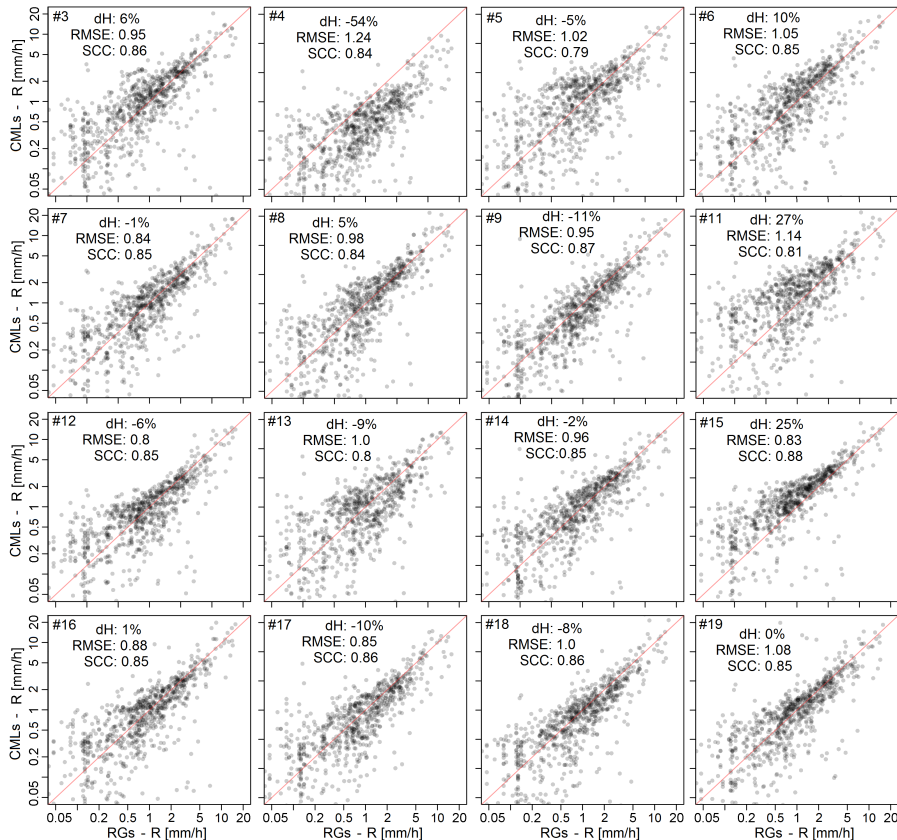


Figure 6.3: Scatter plots comparing rain gauge data (RGs) with CML QPEs for the V model with the same parameters used for all the CMLs (obtained by optimizing for all CMLs at once). Note that the axes are in logarithmic scales. The presented 15-minute data from the 28 rainfall events used for the evaluation represent 349 hours of observations. In 835 out of the 1,401 time steps, rain gauge data contain non-zero records.

6.3.3 WAA model parameters

We also present parameter values used for the WAA model evaluation, both optimized during calibration and taken from the literature (Fig. 6.4). Optimized parameter values of the V and KR-alt models are similarly located in their parameter spaces. Moreover, optimal parameter values for the three various frequency bands are, for these two models, located very close to the optimal values obtained when calibrating for all CMLs at once. This stands in contrast to the V-alt method for which a dependence between the frequency band and the optimal parameter values can be seen. For the KR model, the clear dependence of the two model parameters is most striking. For the S model, optimal values of the W parameter are similar to the parameter values of the O model. However, there is no clear relation to the CML frequency for either of these two WAA models. Parameter values taken from the literature are, in all four cases, located relatively close to the optimized parameters.

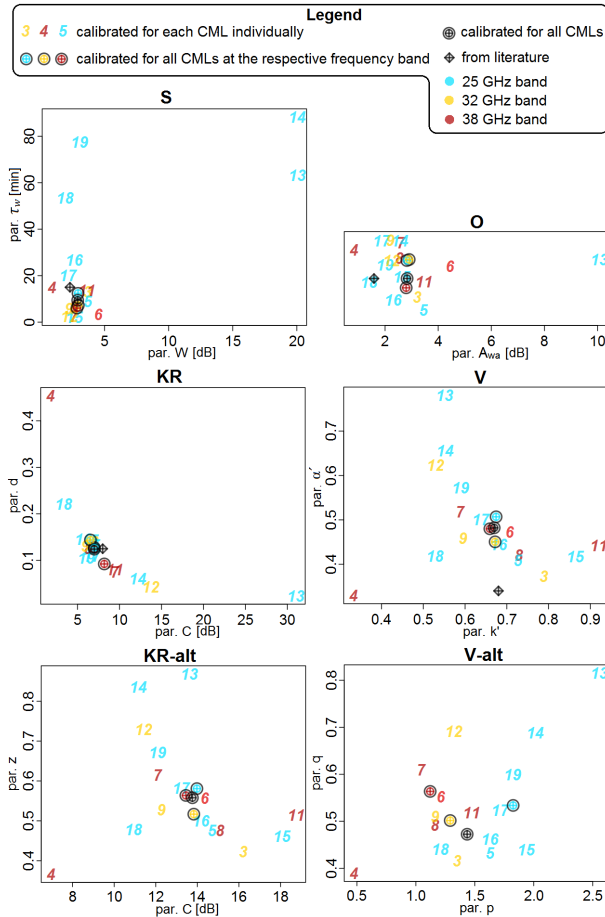


Figure 6.4: WAA model parameter values used for WAA model evaluation, both optimized during calibration and taken from literature (if available). The numbers indicate CML IDs and the colors indicate frequency.

6.4 Discussion

The best results, in terms of dH and RMSE, are, in general, achieved for the models in which WAA A_{wa} is proportional to rainfall intensity R (KR, V, KR-alt, V-alt). For these models, QPEs of the same high quality can be obtained when calibrating for each CML separately. However, the V model and the newly proposed KR-alt model, which both relate A_{wa} to R explicitly, perform very well, even when using the same parameter set for all CMLs. As the KR model relates A_{wa} to A , which is dependent on CML path length, it performs markedly worse when using the same parameter set for more CMLs. The V-alt model performs very well when using the same parameters for CMLs operating at one frequency band and moderately worse when using the same parameter set for all frequency bands. This is in agreement with the calibrated model parameter values (Fig. 6.4) and supports the hypothesis that the parameters of models deriving A_{wa} from R explicitly (V, KR-alt) are more transferrable among CMLs of various frequencies than the parameters of models deriving A_{wa} explicitly from (V-alt).

The results of calibrating the O and S models resemble each other in terms of estimated rainfalls (Fig. 6.1), optimal model parameters (Fig. 6.4), and WAA levels (Fig. 6.5). The rainfall underestimation (i.e. WAA overestimation) associated with the O and S models is likely caused by different optimal parameter values for $RMSE$, used as the calibration objective function, and dH due to the systematic errors in rainfall estimates when modelling WAA A_{wa} as completely or almost constant.

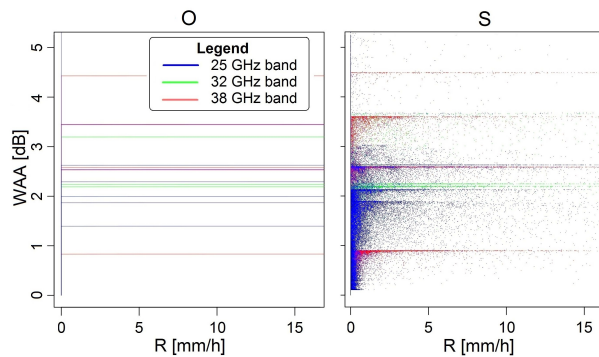


Figure 6.5: WAA levels obtained using the O and S WAA models when calibrated separately for each CML in relation to the respective CML QPEs. The vertical line in the left panel at $R = 0 \text{ mm/h}$ is caused by the nature of the O model. If observed attenuation A is lower than a given parameter value of the O model, WAA is considered equal to A , i.e. there is no rainfall observed.

In total, our results show that unbiased CML QPEs could be retrieved without the need for extensive additional rainfall monitoring when empirical models for WAA estimation are calibrated to rainfall data from the permanent municipal

rain gauge network. Models in which WAA is dependent on rainfall intensity provide the best WAA estimates. Moreover, models explicitly relating WAA to rainfall intensity can provide optimal results even when using the same set of parameter values for CMLs of different characteristics.

The presented results confirm the importance of appropriately correcting for WAA when deriving QPEs from CMLs which is in agreement with previous research (Chwala & Kunstmann, 2019). In particular, the results imply that modelling WAA as constant (O model) is not satisfying when *TRSL* data in 1-min resolution are available. This is in accordance with Pastorek et al. (2019b); Fencl et al. (2019) and contradicting Ostrometzky et al. (2018), however, it should be noted that the latter study focused on WAA estimation for purposes of CML network design and investigated E-band CMLs. Nonetheless, our findings do not dispute the statement that this approach may be a reasonable choice if only 15-min TRSL maxima and minima are available (Chwala & Kunstmann, 2019).

It is shown that the most accurate rainfall estimates are associated with models relating WAA to rainfall intensity, which is in agreement with the WAA estimation approaches presented in Valtr et al. (2019); Kharadly & Ross (2001); Leijnse et al. (2008); Fencl et al. (2019). On the other hand, having provided a comparison of the performance of different WAA models, Schleiss et al. (2013) came to different conclusions. Although their results correspond to ours in terms of *RMSE*, not only for the scenario without WAA correction (Zero; 3.15 mm/h), but also for the WAA models O (1.34 mm/h) and KR (0.91 mm/h), they observed the best performance for the time-dependent S model (0.72 mm/h). It should be noted that they used data from only a single CML and that the parameter values differed from those used in our study because the models were calibrated to local rainfall data from five disdrometers along the CML path. Since, in our case, the S model has only performed (and generally behaved) very similarly as the constant O model, it seems that, in accordance with van Leth et al. (2018), wetting dynamics play a much smaller role for the antennas used in this study than for those analyzed by Schleiss et al. (2013). Recently, similar behavior was observed by Graf et al. (2020) who found that a semi-empirical WAA model assuming a homogeneous water film on antenna radomes dependent on rain rate through a power law (Leijnse et al., 2008) led to more precise CML QPEs than the S model. As their analysis was based on a large country-wide dataset of around 4000 CMLs, it can be concluded that CML antennas for which WAA is not affected by the wetting dynamics are rather usual.

However, the relevance of our findings for other CML networks should be subject to further research. Firstly, it is likely that the capacity of rainfall data from rain gauge networks for calibrating WAA models will depend on gauge network density as the correlation among the gauges decreases with increasing distance. Aggregating the data to coarser resolutions for the

calibration might improve the results as it would improve the correlation (Villarini et al., 2008). Nevertheless, if the sensors are too far from each other, it might be more appropriate to use long-term (e.g. monthly) precipitation heights.

Secondly, the reference areal rainfall used to evaluate the performance of the WAA models has been derived from the same three rain gauges that had been previously used to calibrate the WAA models. However, the rain gauge network density of one gauge per $20\text{--}25\text{ km}^2$ might not be sufficient to reliably represent areal rainfall for events with high spatial variability, e.g. storms with small convective cells. Therefore, out of the 28 individual rainfall events used for the WAA model evaluation, we have identified 11 events with the highest variability among the rain gauges and repeated our analysis using only the data from the remaining 17 events. Differences between the results for the 17 events and for all 28 events together are subtle. The estimated rainfall heights are slightly higher when evaluating all 28 events together than when using the 17 less variable events only. However, differences in terms of RMSE and SCC are minimal, and mutual relations of the individual WAA models and calibration scenarios are not affected.

Due to the use of only three rain gauges, we are also not able to precisely estimate rainfall starts and ends specifically for each CML. Therefore, the process of wet period identification has been designed to avoid classifying wet timesteps as dry, rather than vice versa. This approach makes wet periods longer, however, as the baseline is relatively stable (Schleiss et al., 2013), the order of errors in the estimated baseline levels is well below 1 dB.

Next, all CMLs used in this study are from the same product family of the same manufacturer (Ericsson, Mini-Link) and have aged similarly due to exposure to similar climatic conditions. However, different behavior might be observed for CML antenna hardware of different producers, exposed to different climates for different time periods, or for other specific conditions (e.g. non-zero antenna elevation angles), and thus, the results of this study might not be directly applicable in such circumstances.

Lastly, it should be noted that the V model was originally derived (Valtr et al., 2019) by using one of our 16 CMLs and data from one of the three summer seasons that we have investigated herein.

6.5 Conclusions

We have shown in this study that virtually unbiased QPEs could be retrieved from CMLs without the need for dedicated rainfall monitoring campaigns. CML QPEs with a bias lower than 5% and *RMSE* of 1 mm/h in the median

have been obtained when the empirical models for WAA estimation have been calibrated to rainfall data from the permanent municipal rain gauge network with a spatial resolution of one gauge per 20–25 km². It has been shown that such high-quality QPEs can even be derived from short, sub-kilometer CMLs where WAA is relatively large compared to raindrop attenuation. Models relating WAA to rainfall intensity, implicitly or explicitly, have led to the best results. For the latter, parameter sets have been found to be suitable for CMLs of various path lengths operating at various frequency bands, which could thus be transferred to other locations with CMLs of similar antenna hardware characteristics. Moreover, it has been demonstrated how these WAA models can be successfully applied without any auxiliary rainfall observations, i.e. using CML data only.

This study has confirmed both the potential of CMLs as a source of high-quality rainfall data and the importance of appropriate WAA correction when deriving the QPEs. The presented advances in minimizing the requirements on auxiliary data necessary, both during the calibration of WAA models and during their implementation in the CML data processing routine, represent a legitimate step towards the retrieval of reliable QPEs from large CML networks in conditions where rainfall data are scarce. However, since the potential usefulness of CML QPEs increases with the decreasing availability of other rainfall (or other reference) data, further studies are needed, ideally with extensive datasets containing different CML hardware, to advance our capacity to correct for WAA in the data-scarce conditions. This would also be greatly beneficial for the application of CML QPEs in quantitative hydrological tasks such as urban rainfall-runoff predictions.

Chapter 7

On the value of CML QPEs for urban rainfall-runoff modelling: The final study

7.1 Methods

7.1.1 Performance assessment

?? We have decided to employ, apart from the two mentioned above, as well a metric which combines them – the interval score S_α as formulated by Gneiting & Raftery (2007).

Chapter 8

Dummy chapter

This is the analysis.

```
summary(cars)

##      speed         dist
##  Min.   : 4.0   Min.   :  2.00
##  1st Qu.:12.0   1st Qu.: 26.00
##  Median :15.0   Median : 36.00
##  Mean    :15.4   Mean    : 42.98
##  3rd Qu.:19.0   3rd Qu.: 56.00
##  Max.    :25.0   Max.    :120.00
```


Chapter 9

Conclusion

Lorep ipsum ?

Bibliography

- Anagnostou, E. N., Krajewski, W. F., & Smith, J. (1999). Uncertainty Quantification of Mean-Areal Radar-Rainfall Estimates. *Journal of Atmospheric and Oceanic Technology*, 16(2), 206–215.
- Atlas, D. & Ulbrich, C. W. (1977). Path- and Area-Integrated Rainfall Measurement by Microwave Attenuation in the 1–3 cm Band. *Journal of Applied Meteorology*, 16(12), 1322–1331.
- Berne, A., Delrieu, G., Creutin, J.-D., & Obled, C. (2004). Temporal and spatial resolution of rainfall measurements required for urban hydrology. *Journal of Hydrology*, 299(3-4), 166–179.
- Borup, M., Grum, M., Linde, J. J., & Mikkelsen, P. S. (2016). Dynamic gauge adjustment of high-resolution X-band radar data for convective rain storms: Model-based evaluation against measured combined sewer overflow. *Journal of Hydrology*, 539, 687–699.
- Bourgin, F., Andréassian, V., Perrin, C., & Oudin, L. (2015). Transferring global uncertainty estimates from gauged to ungauged catchments. *Hydrology and Earth System Sciences*, 19(5), 2535–2546.
- Box, G. E. & Cox, D. R. (1964). An analysis of transformations. *Journal of the Royal Statistical Society. Series B (Methodological)*, (pp. 211–252).
- Brauer, C. C., Overeem, A., Leijnse, H., & Uijlenhoet, R. (2016). The effect of differences between rainfall measurement techniques on groundwater and discharge simulations in a lowland catchment: Rainfall Measurement Techniques for Hydrological Simulations. *Hydrological Processes*, 30(21), 3885–3900.
- Breinholt, A., Møller, J. K., Madsen, H., & Mikkelsen, P. S. (2012). A formal statistical approach to representing uncertainty in rainfall–runoff modelling with focus on residual analysis and probabilistic output evaluation—Distinguishing simulation and prediction. *Journal of hydrology*, 472, 36–52.
- Cazzaniga, G., De Michele, C., Deidda, C., D’Amico, M., Ghezzi, A., Nebuloni, R., & Sileo, A. (2020). Calculating the hydrological response of a mountain catchment

9. Conclusion

- using conventional and unconventional (CML) rainfall observations: The case study of Mallero catchment. In *EGU General Assembly 2020* (pp. EGU2020–16368).
- Chwala, C., Gmeiner, A., Qiu, W., Hipp, S., Nienaber, D., Siart, U., Eibert, T., Pohl, M., Seltmann, J., Fritz, J., & Kunstmann, H. (2012). Precipitation observation using microwave backhaul links in the alpine and pre-alpine region of Southern Germany. *Hydrology and Earth System Sciences*, 16(8), 2647–2661.
- Chwala, C., Keis, F., & Kunstmann, H. (2016). Real-time data acquisition of commercial microwave link networks for hydrometeorological applications. *Atmospheric Measurement Techniques*, 9(3), 991–999.
- Chwala, C. & Kunstmann, H. (2019). Commercial microwave link networks for rainfall observation: Assessment of the current status and future challenges. *Wiley Interdisciplinary Reviews: Water*, 6(2), e1337.
- D'Amico, M., Manzoni, A., & Solazzi, G. L. (2016). Use of Operational Microwave Link Measurements for the Tomographic Reconstruction of 2-D Maps of Accumulated Rainfall. *IEEE Geoscience and Remote Sensing Letters*, 13(12), 1827–1831.
- de Vos, L., Leijnse, H., Overeem, A., & Uijlenhoet, R. (2017). The potential of urban rainfall monitoring with crowdsourced automatic weather stations in Amsterdam. *Hydrology and Earth System Sciences*, 21(2), 765–777.
- Del Giudice, D., Albert, C., Rieckermann, J., & Reichert, P. (2016). Describing the catchment-averaged precipitation as a stochastic process improves parameter and input estimation. *Water Resources Research*, 52(4), 3162–3186.
- Del Giudice, D., Honti, M., Scheidegger, A., Albert, C., Reichert, P., & Rieckermann, J. (2013). Improving uncertainty estimation in urban hydrological modeling by statistically describing bias. *Hydrology and Earth System Sciences*, 17, 4209–4225.
- Deletic, A., Dotto, C., McCarthy, D., Kleidorfer, M., Freni, G., Mannina, G., Uhl, M., Henrichs, M., Fletcher, T., Rauch, W., Bertrand-Krajewski, J., & Tait, S. (2012). Assessing uncertainties in urban drainage models. *Physics and Chemistry of the Earth, Parts A/B/C*, 42–44, 3–10.
- Disch, A., Scheidegger, A., Wani, O. F., & Rieckermann, J. (2019). Impact of different sources of precipitation data on urban rainfall-runoff predictions: A comparison of rain gauges, commercial microwave links and radar. *Rainfall monitoring, modelling and forecasting in urban environments. UrbanRain18: 11th International Workshop on Precipitation in Urban Areas. Conference Proceedings*.
- Dotto, C. B., Mannina, G., Kleidorfer, M., Vezzaro, L., Henrichs, M., McCarthy, D. T., Freni, G., Rauch, W., & Deletic, A. (2012). Comparison of different uncertainty techniques in urban stormwater quantity and quality modelling. *Water research*, 46, 2545–2558.
- Einfalt, T., Arnbjergnielsen, K., Golz, C., Jensen, N., Quirmbach, M., Vaes, G., & Vieux, B. (2004). Towards a roadmap for use of radar rainfall data in urban drainage. *Journal of Hydrology*, 299(3-4), 186–202.
- Ericsson (2016). Ericsson Microwave Outlook. Trends and needs in the microwave industry. <https://www.ericsson.com/assets/local/microwave-outlook/documents/ericsson-microwave-outlook-report-2016.pdf>.

- Fencl, M., Dohnal, M., Rieckermann, J., & Bareš, V. (2017). Gauge-adjusted rainfall estimates from commercial microwave links. *Hydrology and Earth System Sciences*, 21(1), 617–634.
- Fencl, M., Dohnal, M., Valtr, P., Grabner, M., & Bareš, V. (2020). Atmospheric observations with E-band microwave links – challenges and opportunities. *Atmospheric Measurement Techniques*, 13(12), 6559–6578.
- Fencl, M., Rieckermann, J., Schleiss, M., Stránský, D., & Bareš, V. (2013). Assessing the potential of using telecommunication microwave links in urban drainage modelling. *Water Science & Technology*, 68.
- Fencl, M., Rieckermann, J., Sýkora, P., Stránský, D., & Bareš, V. (2015). Commercial microwave links instead of rain gauges: Fiction or reality? *Water Science and Technology*, 71(1), 31–37.
- Fencl, M., Valtr, P., Kvičera, M., & Bareš, V. (2019). Quantifying Wet Antenna Attenuation in 38-GHz Commercial Microwave Links of Cellular Backhaul. *IEEE Geoscience and Remote Sensing Letters*, 16(4), 514–518.
- Fenia, F., Pfister, L., Kavetski, D., Matgen, P., Iffly, J.-F., Hoffmann, L., & Uijlenhoet, R. (2012). Microwave links for rainfall estimation in an urban environment: Insights from an experimental setup in Luxembourg-City. *Journal of Hydrology*, 464–465, 69–78.
- Gharesifard, M., Wehn, U., & van der Zaag, P. (2017). Towards benchmarking citizen observatories: Features and functioning of online amateur weather networks. *Journal of Environmental Management*, 193, 381–393.
- Gires, A., Onof, C., Maksimovic, C., Schertzer, D., Tchiguirinskaia, I., & Simoes, N. (2012). Quantifying the impact of small scale unmeasured rainfall variability on urban runoff through multifractal downscaling: A case study. *Journal of Hydrology*, 442–443, 117–128.
- Gneiting, T. & Raftery, A. E. (2007). Strictly proper scoring rules, prediction, and estimation. *Journal of the American Statistical Association*, 102, 359–378.
- Goldshtein, O., Messer, H., & Zinevich, A. (2009). Rain Rate Estimation Using Measurements From Commercial Telecommunications Links. *IEEE Transactions on Signal Processing*, 57(4), 1616–1625.
- Gosset, M., Kunstmann, H., Zougmore, F., Cazenave, F., Leijnse, H., Uijlenhoet, R., Chwala, C., Keis, F., Doumounia, A., Boubacar, B., Kacou, M., Alpert, P., Messer, H., Rieckermann, J., & Hoedjes, J. (2016). Improving Rainfall Measurement in Gauge Poor Regions Thanks to Mobile Telecommunication Networks. *Bulletin of the American Meteorological Society*, 97(3), ES49–ES51.
- Graf, M., Chwala, C., Polz, J., & Kunstmann, H. (2020). Rainfall estimation from a German-wide commercial microwave link network: Optimized processing and validation for 1 year of data. *Hydrology and Earth System Sciences*, 24(6), 2931–2950.
- Haese, B., Hörning, S., Chwala, C., Bárdossy, A., Schalge, B., & Kunstmann, H. (2017). Stochastic Reconstruction and Interpolation of Precipitation Fields Using Combined Information of Commercial Microwave Links and Rain Gauges: RECONSTRUCTION OF RAINFALL FIELDS. *Water Resources Research*, 53(12), 10740–10756.

9. Conclusion

- Harrison, D. L., Scovell, R. W., & Kitchen, M. (2009). High-resolution precipitation estimates for hydrological uses. *Proceedings of the Institution of Civil Engineers - Water Management*, 162(2), 125–135.
- Heistermann, M., Jacobi, S., & Pfaff, T. (2013). Technical Note: An open source library for processing weather radar data (wradlib). *Hydrology and Earth System Sciences*, 17(2), 863–871.
- Honti, M., Stamm, C., & Reichert, P. (2013). Integrated uncertainty assessment of discharge predictions with a statistical error model. *Water Resources Research*, 49, 4866–4884.
- Humphrey, M. D., Istok, J. D., Lee, J. Y., Hevesi, J. A., & Flint, A. L. (1997). A New Method for Automated Dynamic Calibration of Tipping-Bucket Rain Gauges. *Journal of Atmospheric and Oceanic Technology*, 14(6), 1513–1519.
- ITU Radiocommunication Sector (2005). Recommendation 838-3: Specific attenuation model for rain for use in prediction methods.
- Kavetski, D., Kuczera, G., & Franks, S. W. (2006). Bayesian analysis of input uncertainty in hydrological modeling: 1. Theory: INPUT UNCERTAINTY IN HYDROLOGY, 1. *Water Resources Research*, 42(3).
- Kendall, M., Stuart, A., & Ord, J. (1994). *The Advanced Theory of Statistics: Distribution Theory (Vol. 1)*. Arnold, London.
- Kennedy, M. C. & O'Hagan, A. (2001). Bayesian calibration of computer models. *Journal of the Royal Statistical Society: Series B (Statistical Methodology)*, 63, 425–464.
- Kharadly, M. M. Z. & Ross, R. (2001). Effect of wet antenna attenuation on propagation data statistics. *IEEE Transactions on Antennas and Propagation*, 49(8), 1183–1191.
- Kidd, C. & Huffman, G. (2011). Global precipitation measurement: Global precipitation measurement. *Meteorological Applications*, 18(3), 334–353.
- Kollo, T. & von Rosen, D. (2006). *Advanced Multivariate Statistics with Matrices*, volume 579. Springer Science & Business Media.
- Leijnse, H., Uijlenhoet, R., & Berne, A. (2010). Errors and Uncertainties in Microwave Link Rainfall Estimation Explored Using Drop Size Measurements and High-Resolution Radar Data. *Journal of Hydrometeorology*, 11(6), 1330–1344.
- Leijnse, H., Uijlenhoet, R., & Stricker, J. N. M. (2007). Rainfall measurement using radio links from cellular communication networks: RAPID COMMUNICATION. *Water Resources Research*, 43(3).
- Leijnse, H., Uijlenhoet, R., & Stricker, J. N. M. (2008). Microwave link rainfall estimation: Effects of link length and frequency, temporal sampling, power resolution, and wet antenna attenuation. *Advances in Water Resources*, 31(11), 1481–1493.
- Lorenz, C. & Kunstmann, H. (2012). The Hydrological Cycle in Three State-of-the-Art Reanalyses: Intercomparison and Performance Analysis. *Journal of Hydrometeorology*, 13(5), 1397–1420.

- Mancini, A., Lebron, R. M., & Salazar, J. L. (2019). The Impact of a Wet S-Band Radome on Dual-Polarized Phased-Array Radar System Performance. *IEEE Transactions on Antennas and Propagation*, 67(1), 207–220.
- Messer, H., Zinevich, A., & Alpert, P. (2006). Environmental monitoring by wireless communication networks. *Science*, 312, 713–713.
- Montesarchio, V., Lombardo, F., & Napolitano, F. (2009). Rainfall thresholds and flood warning: An operative case study. *Natural Hazards and Earth System Sciences*, 9(1), 135–144.
- Moroder, C., Siart, U., Chwala, C., & Kunstmänn, H. (2019). Modeling of Wet Antenna Attenuation for Precipitation Estimation From Microwave Links. *IEEE Geoscience and Remote Sensing Letters*, (pp. 1–5).
- Muste, M., Lee, K., & Bertrand-Krajewski, J.-L. (2012). Standardized uncertainty analysis for hydrometry: A review of relevant approaches and implementation examples. *Hydrological Sciences Journal*, 57(4), 643–667.
- Ochoa-Rodriguez, S., Wang, L.-P., Gires, A., Pina, R. D., Reinoso-Rondinel, R., Bruni, G., Ichiba, A., Gaitan, S., Cristiano, E., van Assel, J., Kroll, S., Murlà-Tuyls, D., Tisserand, B., Schertzer, D., Tchiguirinskaia, I., Onof, C., Willems, P., & ten Veldhuis, M.-C. (2015). Impact of spatial and temporal resolution of rainfall inputs on urban hydrodynamic modelling outputs: A multi-catchment investigation. *Journal of Hydrology*, 531, 389–407.
- Olsen, R., Rogers, D., & Hodge, D. (1978). The aRb relation in the calculation of rain attenuation. *IEEE Transactions on Antennas and Propagation*, 26(2), 318–329.
- Ostrometzky, J., Raich, R., Bao, L., Hansryd, J., & Messer, H. (2018). The Wet-Antenna Effect—A Factor to be Considered in Future Communication Networks. *IEEE Transactions on Antennas and Propagation*, 66(1), 315–322.
- Overeem, A., Leijnse, H., & Uijlenhoet, R. (2011). Measuring urban rainfall using microwave links from commercial cellular communication networks. *Water Resources Research*, 47(12).
- Pastorek, J. (2014). *Návrh a kalibrácia zrážko-odtokového modelu urbanizovaného povodia Praha Letňany v prostredí SWMM [Design and calibration of a dynamic rainfall-runoff model of an urbanized catchment using the SWMM simulator]*. Bachelor Thesis, Czech Technical University in Prague.
- Pastorek, J. (2016). The effect of different rainfall information on uncertainty in urban runoff modelling. Master's thesis, Czech Technical University in Prague.
- Pastorek, J., Fencl, M., & Bareš, V. (2019a). Calibrating microwave link rainfall retrieval model using runoff observations. In *Geophysical Research Abstracts*, volume 21.
- Pastorek, J., Fencl, M., Rieckermann, J., & Bareš, V. (2019b). Commercial microwave links for urban drainage modelling: The effect of link characteristics and their position on runoff simulations. *Journal of Environmental Management*, 251, 109522.

9. Conclusion

- Pastorek, J., Fencl, M., Rieckermann, J., Sýkora, P., Stránský, D., Dohnal, M., & Bareš, V. (2018). Posouzení srážkových dat z mikrovlnných spojů v městském povodí pomocí analýzy nejistot hydrologického modelu [The Evaluation of CML Rainfall Data in Urban Catchment by Means of Hydrologic Model Uncertainty]. *SOVAK: Časopis oboru vodovodů a kanalizací*, 27, 16–22.
- Pastorek, J., Fencl, M., Stránský, D., Rieckermann, J., & Bareš, V. (2017). Reliability of microwave link rainfall data for urban runoff modelling. In *Proceedings of the 14th IWA/IAHR International Conference on Urban Drainage, Prague* (pp. 1340–1343). Prague, Czech Republic.
- Reichert, P. & Schuwirth, N. (2012). Linking statistical bias description to multiobjective model calibration. *Water Resources Research*, 48.
- Rios Gaona, M. F., Overeem, A., Raupach, T. H., Leijnse, H., & Uijlenhoet, R. (2018). Rainfall retrieval with commercial microwave links in São Paulo, Brazil. *Atmospheric Measurement Techniques*, 11(7), 4465–4476.
- Roversi, G., Alberoni, P. P., Fornasiero, A., & Porcù, F. (2020). Commercial microwave links as a tool for operational rainfall monitoring in Northern Italy. *Atmospheric Measurement Techniques*, 13(11), 5779–5797.
- Scheidegger, A. (2012). *adaptMCMC: Implementation of a Generic Adaptive Monte Carlo Markov Chain Sampler*.
- Schilling, W. (1991). Rainfall data for urban hydrology: What do we need? *Atmospheric Research*, 27(1), 5–21.
- Schleiss, M., Rieckermann, J., & Berne, A. (2013). Quantification and Modeling of Wet-Antenna Attenuation for Commercial Microwave Links. *IEEE Geoscience and Remote Sensing Letters*, 10(5), 1195–1199.
- Schütze, M., Campisano, A., Colas, H., Schilling, W., & Vanrolleghem, P. (2004). Real time control of urban wastewater systems - Where do we stand today? *Journal of Hydrology*, 299(3-4), 335–348.
- Sikorska, A. E., Scheidegger, A., Banasik, K., & Rieckermann, J. (2012). Bayesian uncertainty assessment of flood predictions in ungauged urban basins for conceptual rainfall-runoff models. *Hydrology and Earth System Sciences*, 16(4), 1221–1236.
- Smiatek, G., Keis, F., Chwala, C., Fersch, B., & Kunstmann, H. (2017). Potential of commercial microwave link network derived rainfall for river runoff simulations. *Environmental Research Letters*, 12(3), 034026.
- Spekkers, M. H., Kok, M., Clemens, F. H. L. R., & ten Veldhuis, J. A. E. (2013). A statistical analysis of insurance damage claims related to rainfall extremes. *Hydrology and Earth System Sciences*, 17(3), 913–922.
- Stránský, D., Fencl, M., & Bareš, V. (2018). Runoff prediction using rainfall data from microwave links: Tabor case study. *Water Science and Technology*, 2017(2), 351–359.
- Swan, M. (2012). Sensor Mania! The Internet of Things, Wearable Computing, Objective Metrics, and the Quantified Self 2.0. *Journal of Sensor and Actuator Networks*, 1(3), 217–253.

- Tauro, F., Selker, J., van de Giesen, N., Abrate, T., Uijlenhoet, R., Porfiri, M., Manfreda, S., Caylor, K., Moramarco, T., Benveniste, J., Ciraolo, G., Estes, L., Domeneghetti, A., Perks, M. T., Corbari, C., Rabiei, E., Ravazzani, G., Bogena, H., Harfouche, A., Brocca, L., Maltese, A., Wickert, A., Tarpanelli, A., Good, S., Lopez Alcala, J. M., Petroselli, A., Cudennec, C., Blume, T., Hut, R., & Grimaldi, S. (2018). Measurements and Observations in the XXI century (MOXXI): Innovation and multi-disciplinarity to sense the hydrological cycle. *Hydrological Sciences Journal*, 63(2), 169–196.
- Thorndahl, S., Beven, K., Jensen, J., & Schaarsup-Jensen, K. (2008). Event based uncertainty assessment in urban drainage modelling, applying the GLUE methodology. *Journal of Hydrology*, 357(3-4), 421–437.
- Tsihirintzis, V. A. & Hamid, R. (1997). Modeling and Management of Urban Stormwater Runoff Quality: A Review. *Water Resources Management*, 11(2), 136–164.
- Uhlenbeck, G. E. & Ornstein, L. S. (1930). On the theory of the Brownian motion. *Physical review*, 36, 823.
- Valtr, P., Fencl, M., & Bareš, V. (2019). Excess Attenuation Caused by Antenna Wetting of Terrestrial Microwave Links at 32 GHz. *IEEE Antennas and Wireless Propagation Letters*, 18(8), 1636–1640.
- van der Pol, T., van Ierland, E., Gabbert, S., Weikard, H.-P., & Hendrix, E. (2015). Impacts of rainfall variability and expected rainfall changes on cost-effective adaptation of water systems to climate change. *Journal of Environmental Management*, 154, 40–47.
- van Leth, T. C., Overeem, A., Leijnse, H., & Uijlenhoet, R. (2018). A measurement campaign to assess sources of error in microwave link rainfall estimation. *Atmospheric Measurement Techniques*, 11(8), 4645–4669.
- Vezzaro, L. & Grum, M. (2014). A generalised Dynamic Overflow Risk Assessment (DORA) for Real Time Control of urban drainage systems. *Journal of Hydrology*, 515, 292–303.
- Vihola, M. (2012). Robust adaptive Metropolis algorithm with coerced acceptance rate. *Statistics and Computing*, 22, 997–1008.
- Villarini, G., Mandapaka, P. V., Krajewski, W. F., & Moore, R. J. (2008). Rainfall and sampling uncertainties: A rain gauge perspective. *Journal of Geophysical Research*, 113(D11), D11102.
- Vrugt, J. A., ter Braak, C. J. F., Clark, M. P., Hyman, J. M., & Robinson, B. A. (2008). Treatment of input uncertainty in hydrologic modeling: Doing hydrology backward with Markov chain Monte Carlo simulation: FORCING DATA ERROR USING MCMC SAMPLING. *Water Resources Research*, 44(12).
- Wang, L.-P., Ochoa-Rodríguez, S., Onof, C., & Willems, P. (2015). Singularity-sensitive gauge-based radar rainfall adjustment methods for urban hydrological applications. *Hydrol. Earth Syst. Sci.*, 19(9), 4001–4021.
- Wang, L.-P., Ochoa-Rodríguez, S., Simões, N. E., Onof, C., & Maksimović, Č. (2013). Radar–raingauge data combination techniques: A revision and analysis of their suitability for urban hydrology. *Water Science and Technology*, 68(4), 737–747.

9. Conclusion

- Wang, Q., Shrestha, D. L., Robertson, D., & Pokhrel, P. (2012). A log-sinh transformation for data normalization and variance stabilization. *Water Resources Research*, 48.
- Willems, P., Arnbjerg-Nielsen, K., Olsson, J., & Nguyen, V. (2012). Climate change impact assessment on urban rainfall extremes and urban drainage: Methods and shortcomings. *Atmospheric Research*, 103, 106–118.
- Xiang, Y., Gubian, S., Suomela, B., & Hoeng, J. (2013). Generalized Simulated Annealing for Efficient Global Optimization: The GenSA Package for R. *The R Journal*, 5(1).